CHAPTER V

POLYANILINE NANOFIBERS:CHITOSAN NANOCOMPOSITES FOR BIOMEDICAL APPLICATIONS

This embodiment deals with the optimization and characterization of electrically conductive, biocompatible and biodegradable polyaniline nanofibers:chitosan (PAni:Ch) nanocomposites as a substrate for urease immobilization and as cell culture substrates for a breast cancer MDA-MB-231 cell line and a NIH 3T3 fibroblast cell line in order to examine the combined effect of nanofiber structure and surface modification on cell-biomaterial interactions. The nanocomposites were further checked as a conductive scaffold for electrical stimulation of a neuronal model rat pheochromocytoma 12 (PC12) cell line in order to explore the potential of the materials in neural tissue engineering. The surface of chemically synthesized PAni:Ch nanocomposites was modified with glutaraldehyde and glycine N-hydroxysuccinimide (NHS) ester, separately, to incorporate bioactivity for better cell-biomaterial interactions. This chapter embodies the detailed study of several material properties such as electrical conductivity, surface functional groups and their charge character as well as wettability and material stiffness, moderated by surface functionalization and chitosan (Ch) composite formation to improve cell adhesion, spreading, and growth on conductive polyaniline (PAni) based biomaterials.

5.1 Introduction

Any material for biomedical applications essentially should be biocompatible and bioactive to support the normal functions of biological systems. The final application is determined the specific ability of the material to perform any desired biological event viz. an artificial extracellular matrix (ECM) in tissue engineering, a transducer in biosensors etc. Particularly, tissue engineering focuses on regeneration of lost or damaged tissues with the help of biomaterial scaffolds, cells, and growth factors [85-87]. The biomaterial scaffold should mimic the structure and biological function of

native ECM) as much as possible, both in terms of chemical composition and physical structure. Several parameters such as surface hydrophilicity, wettability, mechanical stiffness, elasticity, electrical signal and surface topography have been identified as having significant influence over the behavior of seeded cells including migration, differentiation, and structural reorganization [233, 234, 377, 378].

Considerable effort has thus been focused on searching for materials with desired bulk properties and techniques which make clear local cellular interactions with their microenvironment and exploit these interactions to design an ideal scaffold that is able to elicit a desirable cellular response. A polymeric nanofiber nonwoven matrix is one of the most promising biomaterials for use as a native ECM analog because it mimics the well known nanoscaled features of the native ECM [85, 92, 104, 121]. Regarding the electrical properties of cells, electrical signals strongly affect cell behavior, affecting ion influx across the cell membrane, altering the membrane potential and conditioning the intracellular signal transduction pathways [120]. The influence of electrical and electromagnetic fields on cells has also been widely investigated, particularly on cardiac myocytes, neuronal cells, keratinocytes, fibroblasts, and mesenchymal stem cells [120]. Conducting polymers (CPs) allow excellent control of the electrical stimulus, possess very good electrical and optical properties, have a high conductivity/weight ratio and can be made biocompatible, biodegradable and porous [120, 196]. Furthermore, the chemical, electrical and physical properties of CPs can be tailored to a specific application by incorporating antibodies, enzymes and other biological moieties [196]. Apart from tissue engineering applications, CPs are also promising materials for biosensing due to direct electron transfer between an enzyme and a polymer. The dramatic changes in the optical, electrical and magnetic properties in nano-dimension as well as the ability of the nanomaterials to mimic the structural feature of biologically important parts, have further pushed the applicability of CP based nanostructures as biomaterials.

Polyaniline (PAni) is one of the most adaptive CPs due to its diverse structural forms, ease of synthesis, high environmental stability and excellent charge transport property by the doping/dedoping process [45, 49, 379, 380]. One of the major advantages of PAni is its solubility in a few selected organic solvents, which makes possible it to process in free standing film form with higher degree of stability on account of insolubility in most of the solvents including water [210]. The *in vitro* biocompatibility of pure PAni or it derivatives has been investigated with various cell

types including H9c2 cardiac myoblasts [157], C2C12 myoblasts [256], L929 murine fibroblasts [381, 382], human mesenchymal stromal cells [383], rat nerve stem cells [381], PC12 cells [381, 384] etc. However, issues such as biocompatibility, biodegradability including any unexpected side effects related to bioactivity are important when considering biomedical applications for these materials. Recently, to overcome the poor biodegradability and biocompatibility, PAni has been blended with natural and synthetic biopolymers for various biomedical applications including tissue engineering, biosensing and drug delivery [381]. If processed all these properties, PAni based materials have the potential to fulfill the technological expectations for biomedical applications.

As a chemical/physical cue, surface functionalization of biomaterials offers a rational and potentially highly efficient approach for regulating cellular function [196, 233, 234]. Surface functionalization and interfacial engineering of polymeric materials can be used to endow the surface with properties which promote cell adhesion, proliferation, and maintain normal cell phenotype and function through favorable interaction with biomolecules present on the cell surface. The most important parameter influencing cell biomaterial interaction through adsorption of proteins is surface hydrophilicity, which in fact allows covalent attachment of proteins on the material surface [233, 234, 366, 377, 378]. CPs are often considered inert synthetic hydrophobic materials. Therefore, it is necessary to increase the hydrophilicity of the surface of CPs and this can be achieved through incorporation of polar groups such as hydroxyl, carboxylic, aldehyde, amino and sulphate groups on top of a materials' surface by wet chemical surface modification techniques [233, 234].

Chitin, the second most abundant natural polysaccharide with N-acetyl-D-glucosamine monomeric units, is a major structural component in the exoskeleton of arthropods and cell walls of fungi and yeast. Due to its non-solubility to common solvents, a deacetylated derivative chitosan (Ch) is more commonly used and due to its solubility in acidic, neutral, and alkaline solutions, Ch is preferred over chitin for a wide range of applications [385]. Ch promotes cell adhesion, proliferation and differentiation and is also biodegradable, biocompatible, nonantigenic and nontoxic [386]. Due to these properties, Ch is used in a range of fields related to biomedicine and is used as a composite to form hybrid materials for tissue engineered scaffolding,

drug delivery, wound dressings, separation membranes and antibacterial coatings, stent coatings and sensors [385-387].

In this embodiment, PAni nanofibers synthesized by dilute polymerization method have been blended with Ch, a natural biopolymer, at a concentration of 4 % and 6 % (w/v) to confer bioactivity and biodegradability for improved function as biomaterial scaffold. Composites of PAni and Ch have been studied already for immobilization of enzyme in bulk form. However, the nanocomposite of PAni and Ch is still to be explored for enzyme immobilization. Besides, the tissue engineering aspect of PAni:Ch composites has not been investigated till now. Whilst the potential biomedical applications for CPs are known ways in which to improve their physicochemical and biological properties using novel nanocomposite and surface functionalization routes have yet to be studied extensively. Within this study, an electrically conductive PAni:Ch nanocomposite based biodegradable material has been surface functionalized with glutaraldehyde and glycine N-hydroxysuccinimide (NHS) ester, separately, in order to investigate the hypothesis that surface functionalization of these conductive materials will enhance bioactivity and improve cell-biomaterial interactions. The physicochemical properties of PAni:Ch nanocomposites before and after surface functionalization have been studied with the help of various characterization tools viz. SEM, XRD, *I-V* measurement, TGA, FTIR, x-ray photoelectron spectroscopy (XPS), and contact angle measurements. The incorporated bioactivity of the glutaraldehyde functionalized PAni:Ch (GFPAni:Ch) nanocomposites has been evaluated in terms of enzyme activity and kinetics of covalently immobilized urease onto them, which catalyzes hydrolysis of urea. Immobilized urease has found broad applications, such as blood detoxification in artificial kidneys, the removal of urea from beverages and foods in food industry, and the reduction of urea content in effluent treatment in agriculture. Moreover, the immobilization of urease on natural or synthetic membranes, for example, CPs based scaffold, has been reported to design highly selective and sensitive biosensors. The effect of surface functionalization of PAni:Ch nanocomposites on their biological properties has been investigated in terms of blood compatibility by Hemolysis assay, cytotoxicity by MTS proliferation assay with MDA-MB-231 cells along with cell adhesion and spreading by acridine orange/ethidium bromide (AO/EtBr) staining and SEM.

Similarly, the effect of altered surface properties of glycine NHS ester functionalized PAni:Ch (EFPAni:Ch) nanocomposites has been investigated to modulate the blood compatibility by Hemolysis assay, cytotoxicity by MTS proliferation assay with 3T3 fibroblasts and rat neuronal model PC12 cells, cell adhesion, spreading and proliferation by live/dead assay and SEM. Electrically stimulation of PC12 cells through electrically conductive collagen I coated PAni:Ch nanocomposites has been performed to explore the potential of these materials in nerve repairing.

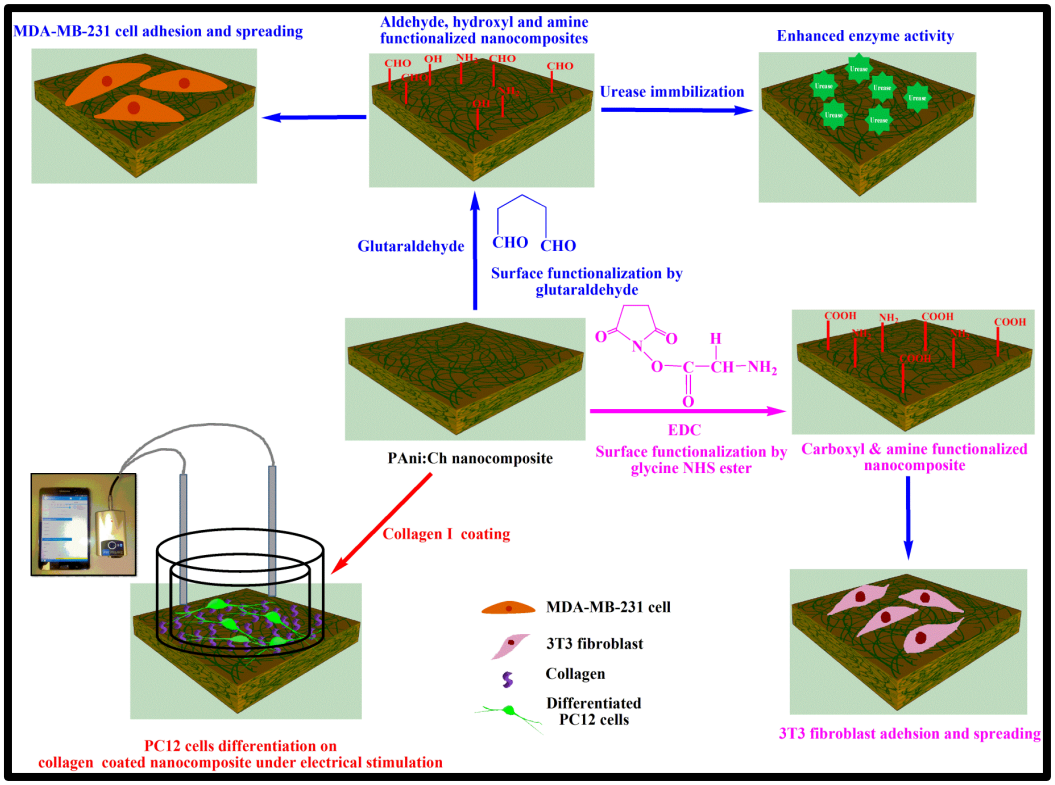

Figure 5.1. Schematic illustration of incorporation of polar functional groups (carboxyl and amine) by surface functionalization of PAni:Ch nanocomposites for improved 3T3 cell adhesion, spreading and proliferation. Electrical stimulation of PC12 cells through collagen coated PAni:Ch nanocomposites for enhanced neurite outgrowth.

It is to be noted that PAni:Ch nanocomposites with 4 wt% and 6 wt% PAni content, have been named as PAni:Ch-4 wt% and PAni:Ch-6 wt%, respectively, throughout the thesis. Consequently, the glutaraldehyde functionalized PAni:Ch nanocomposites with 4 wt% and 6 wt% PAni content, have been named as GFPAni:Ch-4 wt% and

GFPAni:Ch-6 wt%, respectively. Similarly, the glycine NHS ester functionalized PAni:Ch nanocomposites with 4 wt% and 6 wt% PAni content, have been named as EFPAni:Ch-4 wt% and EFPAni:Ch-6 wt%, respectively, throughout the thesis.

The schematic representation of the work carried out in **Chapter V** has been shown in **Figure 5.1**.

5.2 Physicochemical characterization

5.2.1 Electron microscopy

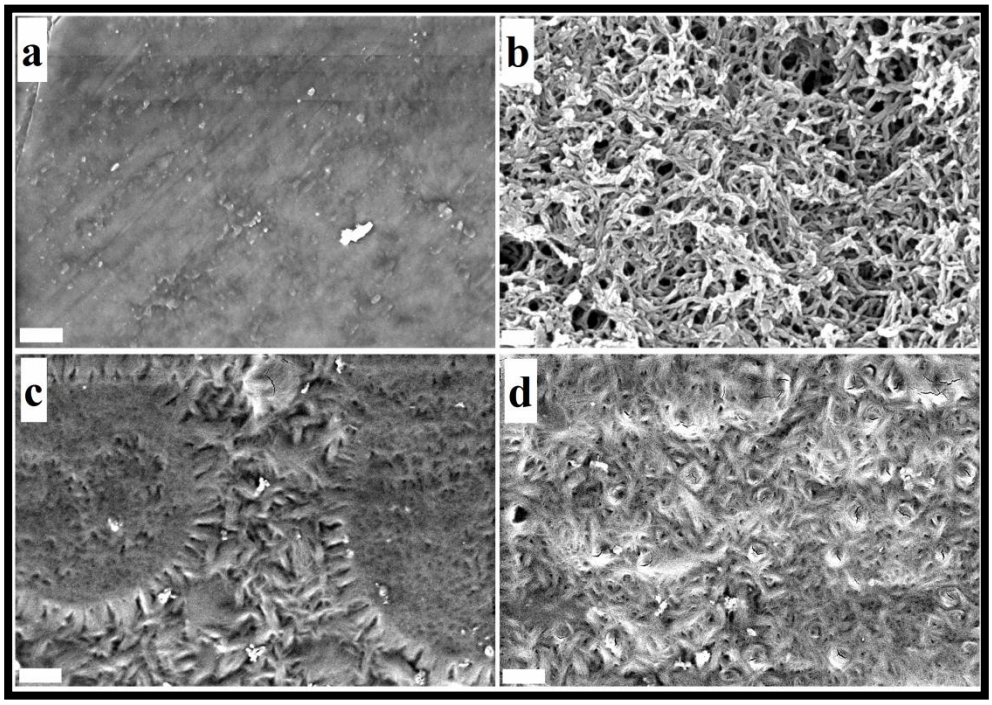

Figure 5.2. Scanning electron micrographs of (a) powdered PAni nanofibers, (b) Ch and PAni:Ch nanocomposites with (c) 4 wt% and (d) 6wt% of PAni content.

Typical SEM micrographs of the PAni nanofibers in powder form [**Figure 5.2 (a)**] demonstrate the nanofibrous structures of PAni with interconnected networks. The SEM micrograph of Ch [**Figure 5.2 (b)**] depicts the smooth and homogeneous surface structure of the Ch film. **Figure 5.2 (c)**&**(d)** reveal layers of interconnected networks of PAni nanofibers soaked in Ch matrix after formation of nanocomposites with 4 wt% and 6 wt% of PAni content, respectively. The surface of the nanocomposites is rough and porous when compared to that of Ch. PAni nanofibers appeared to be

distributed more uniformly in the PAni:Ch nanocomposites with 6 wt% PAni content than in those with 4 wt% PAni content.

5.2.2 X-ray diffraction (XRD) analysis

Figure 5.3 depicts the X-ray diffraction (XRD) patterns of pure Ch, PAni nanofibers and PAni:Ch nanocomposites with varying concentration of PAni nanofibers. The XRD pattern of pure Ch film reveals a broad diffraction peak around 2θ = 22-24°, indicating amorphicity of the biopolymer, which is consistent with the earlier reports [388]. The XRD of powders of PAni nanofibers shows two relatively sharpmajor reflection peaks at 2θ =19° and 25°, suggesting semicrystalline nature of PAni synthesized by dilute polymerization method as discussed in **Chapter IV** [**Section 4.2.1**]. The XRD diffractograms of PAni:Ch nanocomposites films exhibit two broad peaks at 2θ = 15.5° and 22.5° with shoulder at 10.8° in agreement with the characteristic diffractogram of pure Ch as reported earlier [388]. This indicates the enhancement in crystallinity of Ch upon addition of semicrystalline PAni nanofibers. From the XRD patterns of PAni:Ch nanocomposites films with variation of PAni content, it is visible that both the peaks at 2θ =15.5° and 22.5° become sharp with increasing concentration of PAni nanofibers in the nanocomposites.

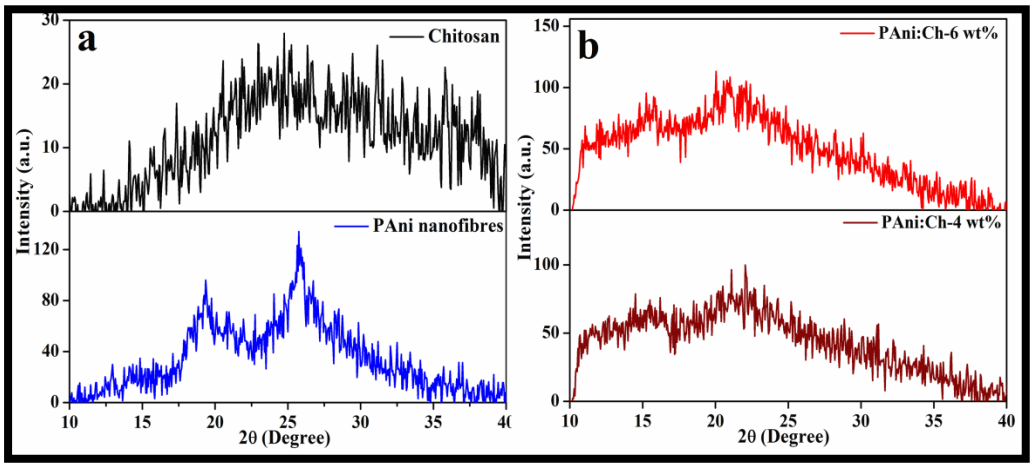

Figure 5.3. (a) X-ray diffraction patterns of pure Ch and PAni nanofibers as labeled; (b) X-ray diffraction patterns of PAni:Ch nanocomposites with 4 wt% and 6 wt% of PAni content as labeled.

Table 5.1. Degree of crystallinity of pure Ch, PAni nanofibers (PNFs) and PAni:Ch nanocomposites with 4 wt% and 6 wt% PAni content.

Sample	Total area	Area of peak at 2θ = 15°-35°	Degree of crystallinity (X_c) %
Ch	604.67	145.76	24.1
PAni	983.45	554.12	56.34
PAni:Ch-4 wt%	671.52	197.88	29.46
PAni:Ch-6 wt%	887.48	287.61	32.4

This observation further suggests the improvement in crystallinity of the nanocomposites with increasing PAni content. The relative percentage of crystallinity of all the materials has been quantified by determining the degree of crystallinity (X_c) using the following formula and presented in **Table 5.1**:

$$X_c = \frac{A_c}{A_c + A_a} \times 100 \qquad 5.1$$

where A_c is the area of the crystalline region and A_a is the area of the amorphous region. The quantitative analysis demonstrates that the incorporation of PAni nanofibers contributes towards the enhancement in the degree of crystallinity of Ch as PAni:Ch-6 wt% has greater degree of crystallinity than that of PAni:Ch-4 wt% [**Table 5.1]**. The enhancement in crystallinity of the nanocomposites with increasing PAni content is attributed to the possible electrostatic interactions between the abundant amino and hydroxyl groups in Ch with the primary and secondary amines of PAni, which probably confer some regularity in the nanocomposites. This predication is consistent with the results reported by Ayad *et al.*[388].

5.2.3 Current-voltage (I-V) characteristics

Figure 5.4 shows the room temperature (300 K) non-linear *I-V* characteristics of pristine PAni:Ch nanocomposites films along with glutaraldehyde functionalized and Glycine NHS ester functionalized nanocomposites films i.e., GFPAni:Ch and EFPAni:Ch nanocomposites with variation in PAni content. The *I-V* characteristics of all the materials are almost symmetric upon reversal of the applied voltage. The *I-V* characteristics the nanocomposites with higher PAni content exhibit higher value of

current at a particular applied voltage, while after surface functionalization both GFPAni:Ch and EFPAni:Ch nanocomposites with different PAni content slight decrease in the current at a particular applied voltage, which may be due to loss in π–π conjugation in PAni chains during surface functionalization process. A better insight into the conduction mechanisms in the materials can be obtained from the log-log plot of the positive side of the corresponding *I-V* data [345].The plots of *I-V* data of the non-functionalized and functionalized nanocomposites in log-log scale along with their fitting according to power law equation $I = KV^m$ indicate two distinct regions in their non-linear *I-V* characteristics [**Figure 5.5 (a-f)]**. At lower voltage region (0<V<4), the *I-V* characteristics is linear, suggesting the conduction mechanism is Ohmic, whereas at higher voltage region (4<V<10), the current varies non-linearly with the applied voltage and hence, it follows SCLC mechanism as discussed in **Chapter IV** [**Section 4.2.3**]. The fitting parameter such as the exponent at lower voltage region (m_1) and at higher voltage region (m_2)along with the critical voltage values for each sample are shown in **Figure 5.5 (a-f).**

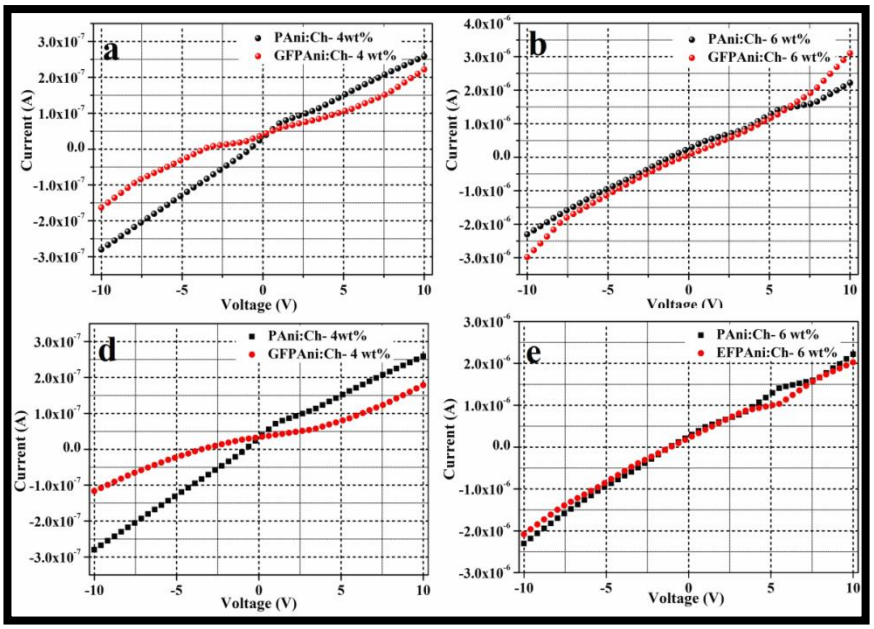

Figure 5.4. Room temperature (300 K) *I-V* characteristics of (a) GFPAni:Ch-4 wt% (red), (b) GFPAni:Ch-6 wt% (red), (c) EFPAni:Ch-4 wt% (red) and (d) EFPAni:Ch-6 wt% (red) with comparison to their non-functionalized counterparts (black).

Table 5.2. Calculated sheet resistance (R_s) and critical voltage (V_c) values of the different PAni:Ch nanocomposites films before and after surface functionalization. Sheet resistance (R_s) data were expressed as Mean ± S.D (n=3).

Sample name	Sheet resistance (R_s) Ω	Critical voltage (V_c) V
PAni:Ch- 4 wt%	$3.64 \pm 1.40 \times 10^7$	3.25
PAni:Ch- 6 wt%	$4.59 \pm 1.65 \times 10^6$	3.10
GFPAni:Ch-4 wt%	$4.81 \pm 0.97 \times 10^7$	3.42
GFPAni:Ch-6 wt%	$5.07 \pm 1.28 \times 10^6$	3.29
EFPAni:Ch-4 wt%	$5.11 \pm 2.03 \times 10^7$	3.41
EFPAni:Ch-6 wt%	$4.86 \pm 1.14 \times 10^6$	3.30

The critical voltage (V_c) values at whichthe transition from Ohmic to non-Ohmic behaviour occurs and the calculated sheet resistance (R_s) values are shown in **Table 5.2**. The critical voltage (V_c) values for PAni:Ch nanocomposites with higher PAni content are less than that of the nanocomposites with lower PAni content, indicating the higher density of free charge carriers in all PAni:Ch-6 wt% before and after functionalization, which results higher value of current at a particular voltage. This observation is further supported by the lower sheet resistance (R_s) values for the nanocomposites with higher PAni content. However, in case of glutaraldehyde functionalized and glycine NHS ester functionalized samples, there is no significant changes in the critical voltage (V_c) are observed and the sheet resistance (R_s) also decreased negligibly after surface functionalization. The results suggest that surface functionalization by glutaraldehyde and glycine NHS ester has no significant impact on the bond conjugation of conducting PAni chains and hence, the nanocomposites films are still conductive after surface functionalization.

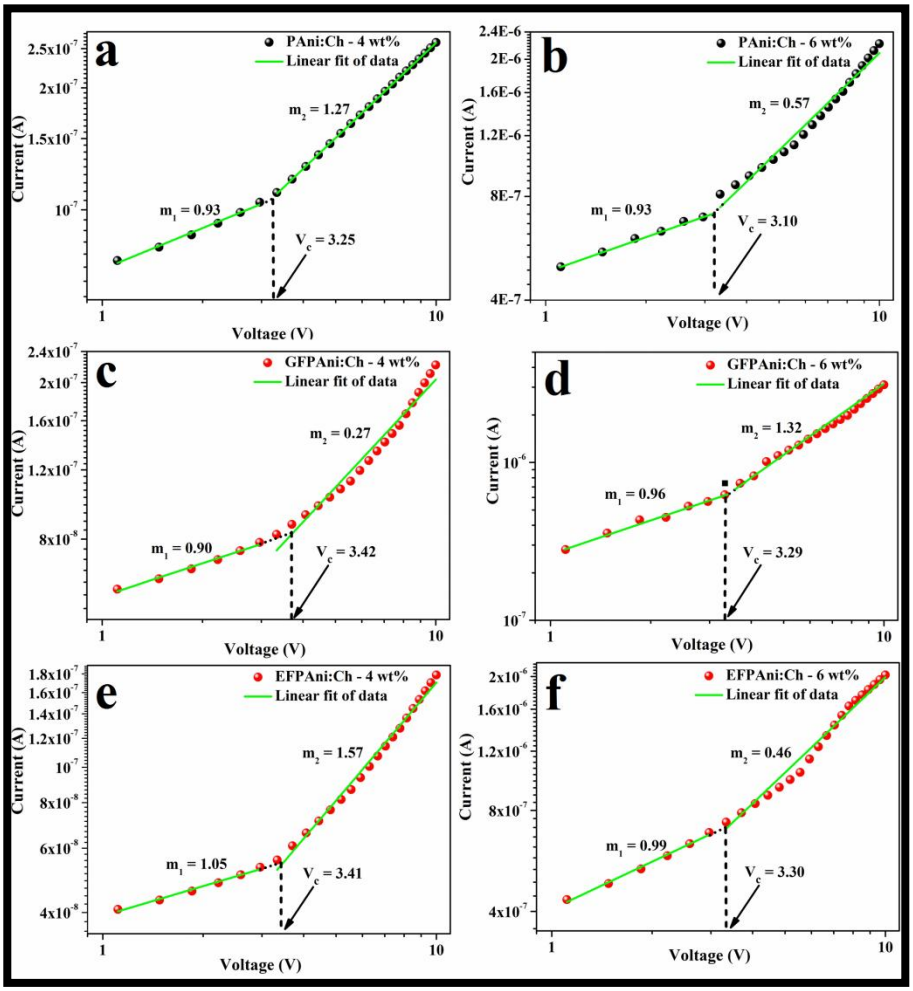

Figure 5.5. Plots of forward I-V data on a log-log scale for (a) PAni:Ch-4 wt%, (b) PAni:Ch-6 wt%, (c) GFPAni:Ch-4 wt%, (d) GFPAni:Ch-6 wt%, (e) EFPAni:Ch-4wt%, and (f) EFPAni:Ch-6 wt%.

5.2.4 Mechanical strength test

Tissues are viscoelastic and are made up of cells and ECM [389]. The cells that make up tissues are adherent, attached to some combination of their neighboring cells and surrounding ECM. Most cells require adhesion for survival termed anchorage dependence and adhere to the ECM through specific anchorage points, termed focal adhesions. These regions localize and concentrate transmembrane adhesion receptors, primarily integrins. As a cell adheres to the substrate through focal adhesions, it pulls on the substrate via its actinomyosin cytoskeleton, senses resistance, and in turn responds to this resistance through the cytoskeleton. It is generally true that cells on stiffer substrates have stiffer, more organized cytoskeletons and more stable focal

adhesions [390, 391]. Hence, the scaffold for tissue regeneration should be mechanically strong enough to support cellular functionality. If the scaffold is mechanically weak, functional tissue regeneration is possible. Therefore, there is an enormous importance to evaluate the mechanical properties of the materials intended for use as biomaterial scaffold.

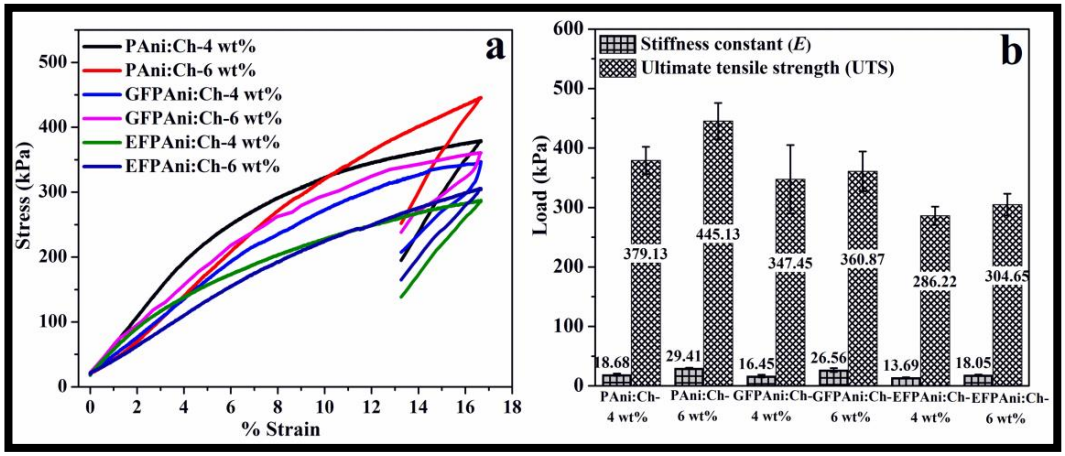

Figure 5.6. (a) Stress *vs* Strain curve and (b) comparison of Young Modulus or stiffness constant (*E*) and ultimate tensile strength (UTS) of PAni:Ch nanocomposites before and after surface functionalization. Data were expressed as Mean ± S.D (n=3).

Figure 5.6 (a) shows the stress *vs.* strain relationship of non-functionalized and functionalized PAni:Ch nanocomposites. The tensile testing provides an indication of the strength and elasticity of the film, which can be reflected by stiffness constant (*E),* tensile strength and elongation at break. The stress *vs.* strain relationship of non-functionalized nanocomposites is better than the functionalized nanocomposites. In case of functionalized nanocomposites, glutaraldehyde functionalized nanocomposites exhibit improved mechanical properties than glycine NHS ester functionalized nanocomposites. It is also evident from **Figure 5.6 (a)** that nanocomposites with higher PAni content has better mechanical properties than the nanocomposites with lower PAni content. In order to compare the mechanical properties of different nanocomposites in quantitative manner, the stiffness constant (*E*) and the ultimate tensile strength (UTS) have been derived from the corresponding stress *vs.* strain data and presented in **Figure 5.6 (b)**. The results reveal that the stiffness constant (*E*) and the UTS of non-functionalized nanocomposites i.e. PAni:Ch- 4wt% (E=18 kPa and

UTS=379 kPa) and Pani:Ch-6 wt% (E=29 kPa and UTS=445 kPa) are greater than that of glutaraldehyde functionalized nanocomposites i.e., GFPAni:Ch-4 wt% (E=16 kPa and UTS=347 kPa) and GFPAni:Ch- 6 wt% (E=26 kPa and UTS=360 kPa) as well as glycine NHS ester functionalized nanocomposites i.e., EFPAni:Ch-4 wt% (E=13 kPa and UTS=286 kPa) and EFPAni:Ch-6 wt% (E=18 kPa and UTS=304 kPa). An increase in PAni nanofibers makes the composite more rigid; since nanocomposites with 6 wt% PAni nanofiber content before and after surface functionalization, have a higher stiffness constant (*E*) as well as UTS than 4 wt% composition of nanocomposites before and after surface functionalization. The decrease in the stiffness constant (*E*) and the UTS after surface functionalization may be due to hydrolysis of the Ch matrix during the surface functionalization step.

The elastic modulus of living tissues varies over many orders of magnitude. Brain, for example, has stiffness constant (*E)* of several hundred pascal, whereas the *E* of muscle is more than 12 kPa and that of tendon and cartilage is in the range of megapascals [392]. Normal liver has an *E* of 300 to 600 Pa, increasing to 20 kPa or higher as fibrosis and cirrhosis develop [392]. The stiffness constant (*E*) of normal lung tissue ranges between 1 and 5 kPa [392]. Fibroblasts achieve maximal spreading at a substrate stiffness of ~10 kPa [393]. Therefore, even though the stiffness constant (*E*) of surface functionalized nanocomposites are lower than that of pristine nanocomposites, they are in a suitable range for most of the tissue function, particularly softer tissues such as nerve and skin.

5.2.5 Stability test

Herein, Ch was used as a biodegradable and biocompatible polymer to confer biodegradability to the nanocomposites with PAni for possible applications as tissue engineered scaffolds. Degradation is essential to avoid subsequent surgical removal of implanted scaffolds [92]. For long-term performance, the implanted scaffolds should be stable enough in terms of electrical and mechanical properties. In the present study, we need the nanocomposites to retain its conductive properties in physiological environment for possible electrical stimulation in nerve regeneration. Hence, the electrical stability and biodegradation of PAni:Ch nanocomposites were accomplished in PBS (pH=7.4) at 37^{o}C for 15 days.

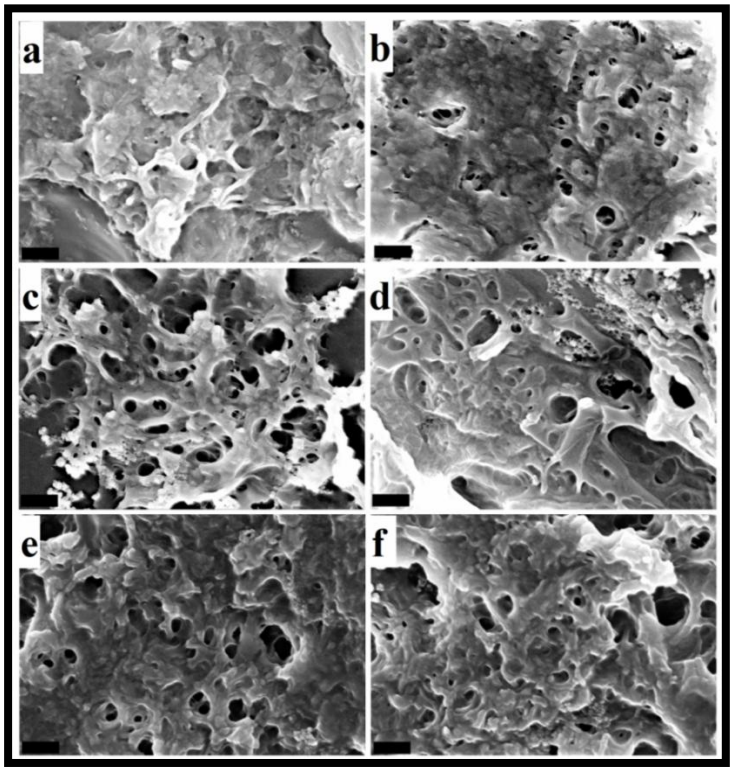

Figure 5.7. Scanning electron micrographs of (a) PAni:Ch-4 wt%, (b) PAni:Ch-6 wt%, (c) GFPAni:Ch-4 wt%, (d) GFPAni:Ch-6 wt%, (e) EFPAni:Ch-4 wt% and (f) EFPAni:Ch-6wt%recorded after keeping in PBS (pH=7.4) for 15 days (Scale bar = 200 nm).

Table 5.3. Sheet resistance (R_s), and percentage of weight loss of the non-functionalized and functionalized PAni:Ch nanocomposites after 15 days in PBS (pH=7.4).

Sample name	Sheet resistance(Ω)		%Weight loss
	Before	After 15 days in PBS	
PAni:Ch-4 wt%	$3.64 \pm 1.40\times10^{7}$	$4.01\pm2.11\times10^{7}$	18.05 ± 3.66
PAni:Ch-6 wt%	$4.59 \pm 1.65\times10^{6}$	$4.89\pm 2.44\times10^{6}$	13.66 ± 2.07
GFPAni:Ch-4 wt%	$4.81\pm0.97\times10^{7}$	$5.39 \pm 1.77\times10^{7}$	21.11± 3.34
GFPAni:Ch-6 wt%	$5.07 \pm 1.28\times10^{6}$	$5.53\pm2.21\times10^{6}$	15.09± 1.57
EFPAni:Ch-4 wt%	$5.11\pm 2.03\times10^{7}$	$6.05 \pm 1.52\times10^{7}$	26.32± 2.42
EFPAni:Ch-6 wt%	$4.86 \pm 1.14\times10^{6}$	$5.22 \pm 2.02\times10^{6}$	19.34± 2.19

SEM images [**Figure 5.7**] of the nanocomposites after incubation in PBS for 15 days shows remarkable enhancement in porous morphology on the surface. The distribution of pore diameters after 15 days of incubation in PBS were increased from 20-100 nm to 50-1000 nm, providing essential porosity of tissue engineered scaffolds. The increase in pore size likely arises from degradation of Ch by hydrolysis, whereas PAni nanofibers in the nanocomposites are expected to be unaffected due to its inert nature. This proposition is supported by the negligible change in sheet resistance of the nanocomposites after 15 days of incubation as presented in **Table 5.3**. There is only slight decrease in sheet resistance values for all the materials. Besides, percentage of weight loss of all the materials has been determined to confirm any degradation occurred if any [**Table 5.3**]. The results indicate that surface functionalized nanocomposites exhibit higher percent of weight loss as compared to non-functionalized nanocomposites. Interestingly, the glycine NHS ester functionalized nanocomposites show highest weight loss, which is in accordance with the fact of utilization of esterification to confer biodegrability of materials [394, 395]. Moreover, it has been also observed that nanocomposites with higher PAni content exhibit less percentage of weight loss. The results suggest that PAni nanofibers play a crucial role in maintaining the electrical and structural stability of the nanocomposites than Ch, which indicates the potential of these nanofibers as a conductive scaffold for tissue engineering applications, particularly for neural tissue engineering.

5.2.6 Thermogravimetric (TGA) analysis

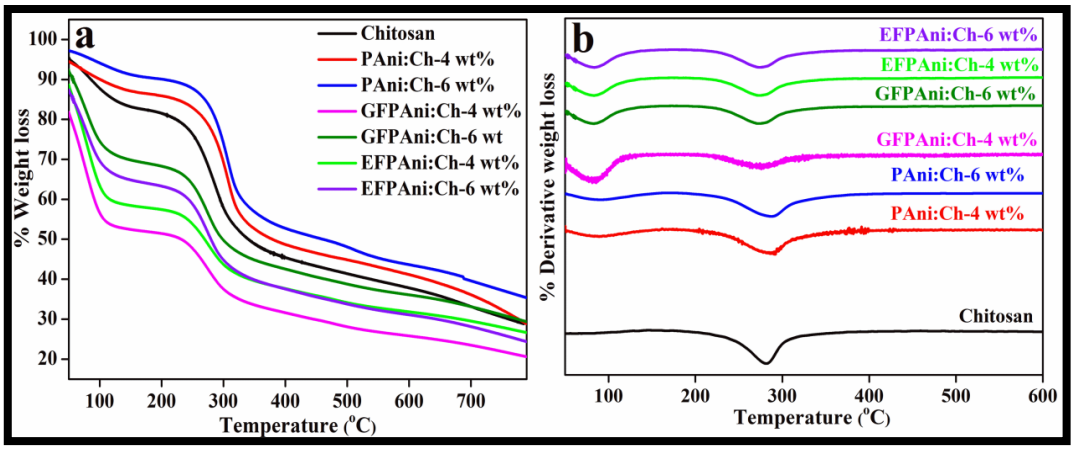

Figure 5.8. (a) TGA thermograms and (b) DTG plots of different PAni:Ch nanocomposites as labeled.

Thermal stability of different PAni:Ch nanocomposites materials have been investigated with the help of thermogravimetric analyzer at a heating rate of 30°C/min under nitrogen atmosphere. The TGA thermograms and DTG plots of non-functionalized and functionalized PAni:Ch nanocomposites are shown in **Figure 5.8 (a) and (b)**.

Table 5.4. Major thermal degradation temperatures and corresponding weight loss of the non-functionalized and functionalized nanocomposites.

Sample name	Major degradation temperature (^oC)	% Weight loss	% Residue at 700^oC
Ch	281	34	33
PAni:Ch- 4wt%	286	25	36
PAni:Ch- 6wt%	288	21	39
GFPAni:Ch- 4wt%	276	56	25
GFPAni:Ch- 6wt%	278	44	33
EFPAni:Ch- 4wt%	275	52	29
EFPAni:Ch- 6wt%	276	47	28

The major decomposition temperatures of different nanocomposites, obtained from the DTG curves and the corresponding weight loss, obtained from the TGA curves, are presented in **Table 5.4**. Ch shows a discrete weight loss at a temperature of 281^oC due to the degradation of the polymer chain [396, 397]. This degradation temperature is shifted towards the higher temperature region in case of the non-functionalized nanocomposites indicating the improvement in thermal stability of the nanocomposites after incorporation PAni nanofibers [**Table 5.4**]. It is further demonstrated by the lower % weight loss at 286-288^oC and higher %Residual weight for the non-functionalized nanocomposites than that of all other materials. However, after surface functionalization, the major degradation temperature is shifted towards slightly lower temperature region and consequently, the %weight lossincreases and %Residual weight decreases [**Table 5.4**]. This indicates decrease in thermal stability of the nanocomposites after surface functionalization. Furthermore, another degradation temperature below 100^oC has been observed in the DTG curves of the functionalized nanocomposites. This degradation temperature can be assigned to the degradation of the functionalizing molecules and loss of moisture from the nanocomposites. However, the characteristic thermal degradation peak for PAni

around 510-520^{o}C has not been observed as discussed in **Chapter IV** [**Section4.2.4**]. The lower concentration of PAni in the nanocomposites is the reason of this.

5.2.7 Surface properties

5.2.7.1 Surface chemistry of glutaraldehyde functionalized PAni:Ch nanocomposites

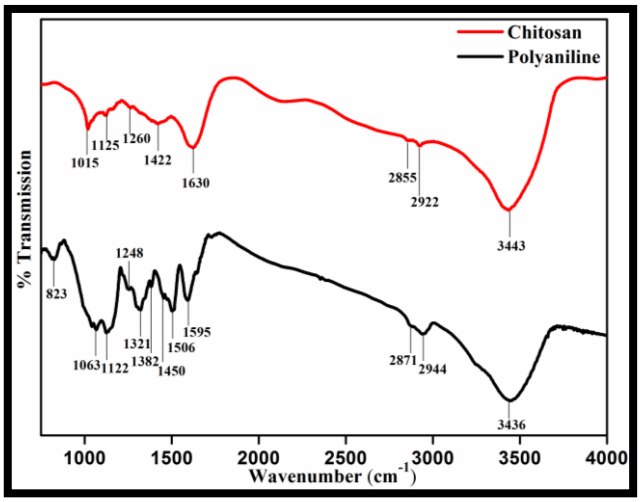

Figure 5.9. Vibrational spectra of PAni nanofibers (black) and pure Ch (red).

The FT-IR spectra of pure PAni and Ch are shown in **Figure 5.9.** The peak appeared at ~823 cm^{-1}in the FT-IR spectrum of PAni is assigned to the C-H out of plane bending vibration of the para disubstituted benzene ring [349-352].The appearance of a band at ~1063 cm^{-1} is attributed to the C-N stretching vibration of the primary amine of the PAni backbone [349-351]. The peaks corresponding to the C-N stretching vibration in the Q=B=Q unit and N-H bending in the –NH_2 of PAni appears at ~1382 and ~1321 cm^{-1}, respectively [349-351]. The vibrational bands in the region ~1450-1506 cm^{-1} and ~1595 cm^{-1} are associated with the C=C stretching vibration of the benzenoid and quinoid unit of the PAni backbone [349-351].The C=N stretching vibration in the quinoid unit of PAni often overlaps in this region [349-351]. The broad vibrational band centered at ~3436 cm^{-1} is assigned to N-H stretching vibration [349-351]. The appearance of the peak at ~1015 cm^{-1} in the FT-IR spectrum of Ch is assigned to O-H bending vibration [349-351]. The bands at ~1125 cm^{-1} and ~1260 cm^{-1} are attributed to the anti-symmetrical stretching vibration of the C-O-C bridge

and the C-N stretching vibration of the secondary aromatic amine of Ch, respectively [349-351]. A strong band at ~1630 cm^{-1} is assigned to C=O stretching in the amide groups (-$NHCOCH_3$-due to partial deacetylation of Ch) [349-351]. Two weak bands appearing at ~2855-2922 cm^{-1} are associated with C-H stretching of aliphatic groups. The broad band centered at ~3443 cm^{-1} is due to O-H & N-H stretching vibration in Ch [349-351].

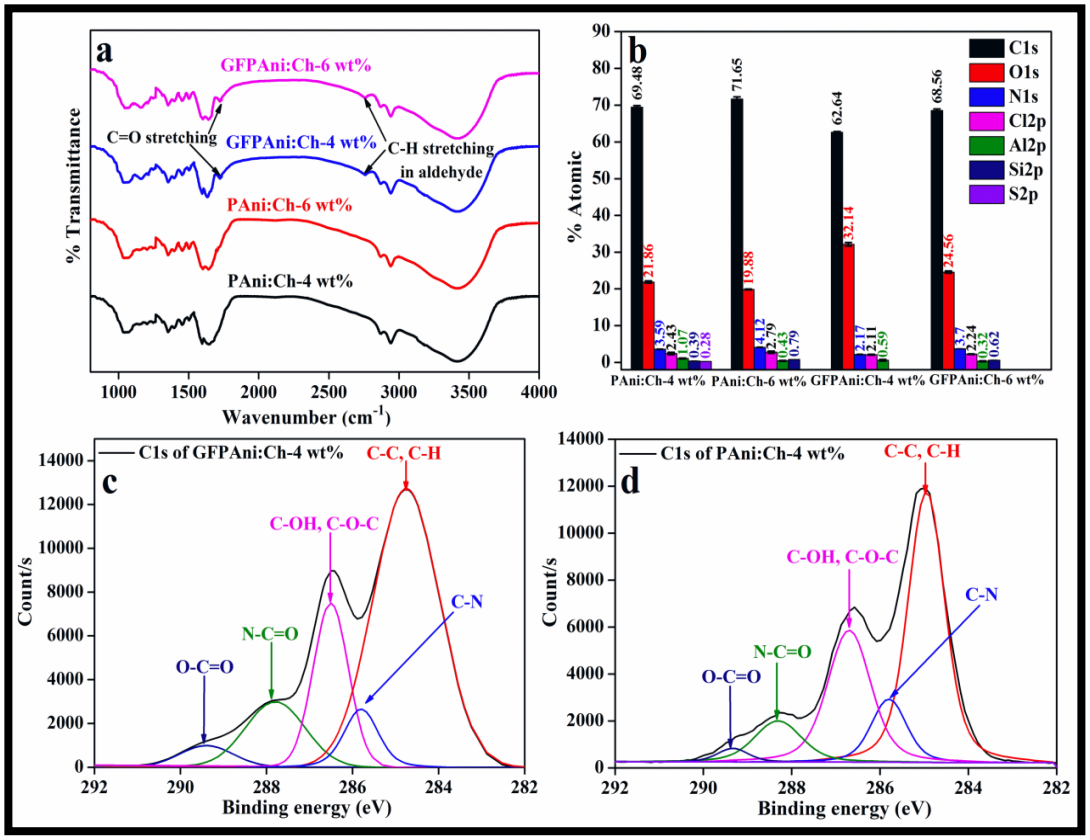

Figure 5.10. (a) Vibrational spectra of PAni:Ch nanocomposites before and after surface functionalization by glutaraldehyde; (b) elemental composition PAni:Ch nanocomposites before and after functionalization with glutaraldehyde. Peak deconvolutions of high-resolution C1s XPS spectra of (c) PAni:Ch-4 wt% and (d) GFPAni:Ch-4 wt%.

The characteristic vibrational bands for both PAni & Ch are observed in the FT-IR spectra of PAni:Ch nanocomposites with slight shifting [**Figure 5.10 (a)]**. The broadening and the shifting of the band around 3450 cm^{-1} of corresponding to O-H & N-H stretching vibration in PAni and Ch indicates electrostatic forces and the

hydrogen bonding between –OH of Ch and -$NH_2$of PAni in PAni:Ch nanocomposites with variation in PAni content [388, 398].

The FT-IR spectra of surface functionalized PAni:Ch nanocomposites show two small but new bands, one for C=O stretching at 1724 cm^{-1} and the other for C-H stretching in aldehyde at 2750cm^{-1}, which confirms the incorporation of aldehyde functionality in the nanocomposites after surface functionalization with glutaraldehyde [**Figure 5.10 (a)]**.

The already present vibrational band for C=O stretching of the secondary amide of partially deacetylated Ch in FT-IR spectra of the non-functionalized nanocomposites are seen to be shifted from 1632-1635 to 1643-1649 cm^{-1} after functionalization with glutaraldehyde [388, 398]. Moreover, the intensity of this band is slightly higher in the FT-IR spectra of the functionalized nanocomposites as compared to the non-functionalized nanocomposites. This indicates possible amide bond formation between the amino group of Ch in PAni:Ch nanocomposites and aldehyde group of monomeric glutaraldehyde. Simultaneously, this can be also C=N stretching vibrations in Schiff base formed between aldehyde group of monomeric glutaraldehyde and primary amine of Ch in the nanocomposites.

Table 5.5. Elemental composition of non-functionalized and glutaraldehyde functionalized PAni:Ch nanocomposites determined by XPS survey scans.

Material	**C1s (%)**	**O1s (%)**	**N1s (%)**	**Cl2p (%)**	**S2p (%)**	**Si2p (%)**	**Al2p (%)**
PAni:Ch-4 wt%	69.48	21.86	3.59	2.43	0.28	0.39	1.07
PAni:Ch-6 wt%	71.65	19.88	4.12	2.79	-	0.79	0.43
GFPAni:Ch-4 wt%	62.64	32.14	2.17	2.11	-	-	0.59
GFPAni:Ch-6 wt%	68.56	24.56	3.7	2.24	-	0.62	0.32

To confirm the preliminary observation obtained by FT-IR analysis, XPS was performed in order to understand the chemical differences in the surfaces of the non-functionalized and functionalized of PAni:Ch nanocomposites. Elemental composition of PAni:Ch nanocomposites before and after functionalization with glutaraldehyde is shown in **Figure 5.10 (b)** and **Table 5.5**. The results indicate increase in the atomic percentage of oxygen (O1s) in both PAni:Ch nanocomposites with variation in PAni content, whereas the presence of S2p, Si2p and Al2p on the

surface could be due to external contamination [**Table 5.5**]. The conductive behaviour of the nanocomposites is supported by the presence of chlorine (Cl2p) on the surface [**Table 5.5**].

Table 5.6. Details of C1s narrow scan spectra of PAni:Ch-4 wt% and GFPAni:Ch-4 wt% corresponding C1s peak deconvolution [366, 399, 400].

Chemical group	PAni:Ch-4 wt%		GFPAni:Ch-4 wt%	
	B. E. (eV)	Atomic (%)	B. E. (eV)	Atomic (%)
C-C, C-H	284.95	49.15	284.80	35.26
C-N	285.80	11.02	285.83	11.86
C-O-C, C-OH	286.70	28.20	286.53	31.67
N-C=O	288.11	9.55	287.90	15.56
O-C=O, C=O	289.34	2.07	289.44	4.64

The high resolution C1s spectra of PAni:Ch-4 wt% and GFPAn:Ch- 4wt% along with their peak deconvolutions are shown in **Figure 5.10 (c) & (d)** and detailed in **Table 5.6**. Here, the most important observation is that the enrichment of the surface of PAni:Ch nanocomposites with higher fractions of N-C=O, C=O and C-OH after functionalization with glutaraldehyde as compared to that of non-functionalized nanocomposites. The higher fraction N-C=O on GFPAni:Ch-4 wt%, which is almost doubled after functionalization, along with the confirmation of higher atomic percentage of oxygen (O1s), confirms the amide bond formation between monomeric glutaraldehyde and the nanocomposites. Similarly, the higher percentage of C=O indicates the free aldehyde (CHO) functionality on the surface of functionalized nanocomposites.

The information obtained by FT-IR and XPS analysis has been used to predict the probable mechanisms of surface functionalization of PAni:Ch nanocomposites by glutaraldehyde. The interaction mechanisms of monomeric glutaraldehyde with the active sites ($-NH_2$ & $-CH_2OH$) of PAni:Ch nanocomposites through amide bond and Schiff base formation are shown in **Figure 5.11**.

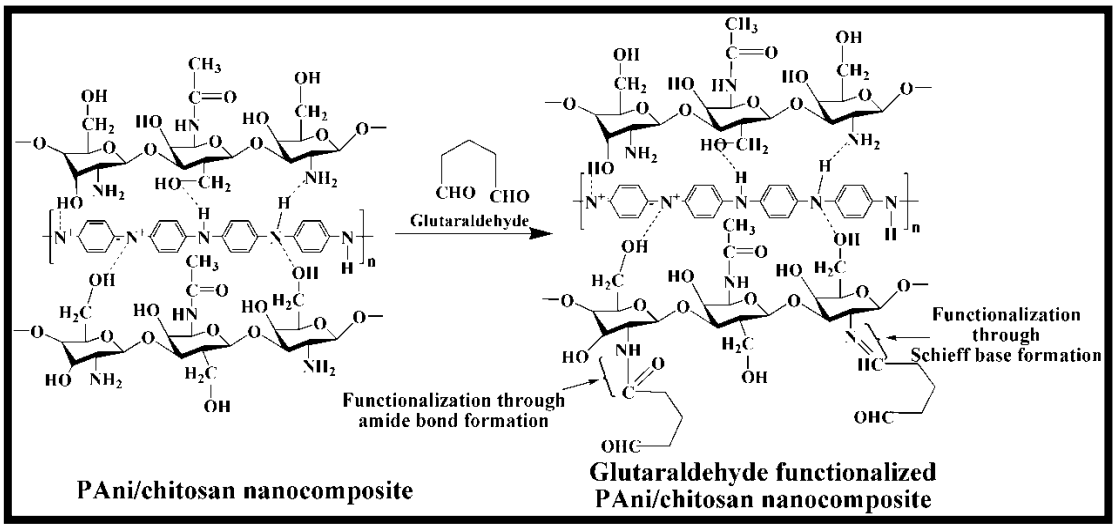

Figure 5.11. Probable interaction mechanisms of glutaraldehyde with PAni:Ch nanocomposites based on XPS and FTIR results.

5.2.7.2 Surface chemistry of glycine NHS ester functionalized PAni:Ch nanocomposites

The FT-IR spectra of pure PAni and Ch are shown in **Figure 5.9** and discussed their observed characteristics vibrational bands in the previous section. **Figure 5.12(a)** shows the FT-IR spectra of the non-functionalized and functionalized PAni:Ch nanocomposites. The spectra of glycine NHS ester functionalized nanocomposites reveal a medium band for C=O stretching at about 1724 cm^{-1} and a broad band centered at about 3017 cm^{-1} corresponding to strongly H-bonded O-H stretching vibration, confirming the certain presence of carboxylic acid [352]. The weak C-O stretching in –COOH can be observed at about 1237 cm^{-1}. The intense and sharp absorption bands at about 1405-1499 cm^{-1} and 1556 cm^{-1} in the spectrum of non-functionalized nanocomposites are assigned to C=C stretching in the benzenoid and quinoid unit of PAni, respectively [349-352]. The spectrum of modified nanocomposites also exhibits similar bands; however, they are weak as compared to the former. The reason may be as follows: The N-H bending of the primary amine of Ch occurs in the region 1556 cm^{-1}. The N-H deformation vibration in $–NH_2$ of Ch appears around 1400 cm^{-1}. During surface functionalization, Ch is expected to be more exposed and the primary amine ($-NH_2$) of Ch actively takes part in surface functionalization processes. The weak band at about 1632 cm^{-1} present in all spectra is

associated with C=O stretching of the secondary amide of partially deacetylated Ch [388, 398]. After surface functionalization, this band is shifted slightly towards a lower frequency as seen in **Figure 5.12(a)**. The spectra of functionalized nanocomposites exhibit two distinct C-N stretching bands in the range 1128-1175 cm^{-1}, whereas the non-functionalized nanocomposites show this band at about 1153 cm^{-1}. Some weak bands around 1290 cm^{-1} can also be attributed to aromatic C-N stretching. The broad vibrational bands observed in the region 3330-3600 cm^{-1} of the spectra of functionalized nanocomposites are associated with N-H stretching in the primary amine region as well as free O-H stretching vibrations.

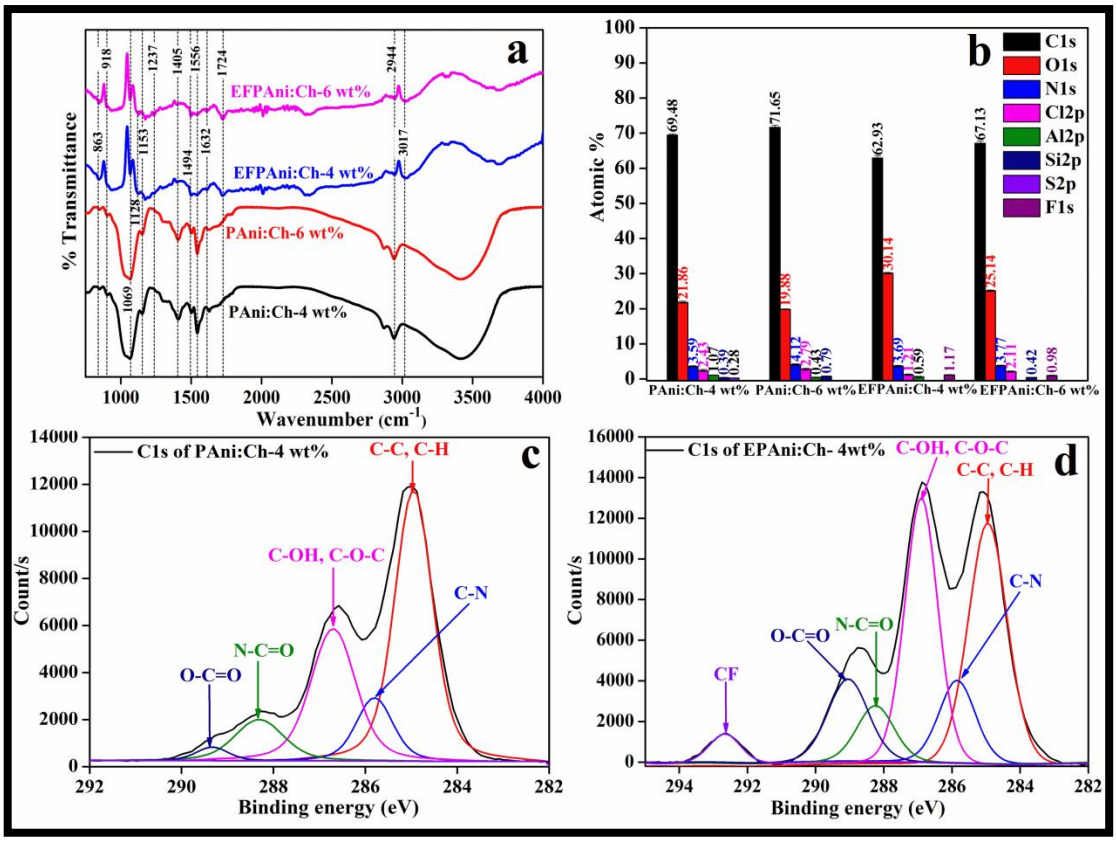

Figure 5.12. (a)Vibrational spectra of PAni:Ch nanocomposites and (b) elemental composition PAni:Ch nanocomposites before and after surface functionalization by glycine NHS ester. Peak deconvolutions of high-resolution C1s XPS spectra of (c) PAni:Ch-4 wt% and (d) EFPAni:Ch-4 wt%.

Table 5.7. Elemental composition of non-functionalized and glycine NHS ester functionalized PAni:Ch nanocomposites determined by XPS survey scans.

Material	C1s (%)	O1s (%)	N1s (%)	Cl2p (%)	S2p (%)	Si2p (%)	Al2p (%)	F1s
PAni:Ch-4 wt%	69.48	21.86	3.59	2.43	0.28	0.39	1.07	-
PAni:Ch-6 wt%	71.65	19.88	4.12	2.79	-	0.79	0.43	-
EFPAni:Ch-4 wt%	62.93	30.14	3.69	1.21	-	-	0.59	1.17
EFPAni:Ch-6 wt%	67.13	25.14	3.77	2.11	-	0.42	-	0.98

XPS analysis was carried out in order to understand the chemical differences before and after surface functionalization of PAni:Ch nanocomposites with 4 wt% PAni content. Chemical composition of the surface of the PAni:Ch nanocomposites before and after surface functionalization by glycine NHS ester was obtained by XPS survey scans and shown in **Figure 5.12(b)** and **Table 5.7**. High resolution C1s narrow scan spectra of PAni:Ch-4 wt% and EFPAni:Ch-4 wt% are shown in **Figure 5.12(c) & (d)** and detailed in **Table 5.8**. The results indicates that the major difference arising after surface functionalization is the nearly six times increase of carboxylic acid components. In addition to the huge increase of carboxylic acid components, the atomic percentage of O1s and N1s are found to be increased up to 30.14% and 3.69% from 21.86% and 3.59%, respectively, after surface functionalization as shown in **Table 5.7**.

Table 5.8. Details of C1s narrow scan spectra of PAni:Ch-4 wt%and EFPAni:Ch-4 wt% and their corresponding C1s peak deconvolutions [366, 399, 400].

Chemical group	PAni:Ch-4 wt%		EFPAni:Ch-4 wt%	
	B. E. (eV)	Atomic (%)	B. E. (eV)	Atomic (%)
C-C, C-H	284.95	49.15	284.95	34.45
C-N	285.80	11.02	285.85	10.86
C-O-C, C-OH	286.70	28.20	286.90	31.67
N-C=O	288.31	9.55	288.25	7.56
O-C=O	289.34	2.07	289.05	12.14
CF2	0	0	292.66	3.33

The enrichment of the surface of PAni:Ch nanocomposites after functionalization by glycine NHS ester with higher fractions of O-C=O, C-OH along with higher percentage of O1s and N1s confirms the incorporation of glycine onto the surface of nanocomposites making it a carboxyl functionalized surface. We also witnessed the presence of –CF2 fractions in the narrow scan XPS data [**Figure 5.12(d)**], which could be a contaminant left over from the trifluoroacetic acid treatment of glycine NHS ester. The presence of Cl2p in functionalized nanocomposites indicates doping level of PAni as found in the elemental composition analysis [**Table 5.8**], whereas the presence of S2p, Si2p and Al2p on the surface of functionalized nanocomposites could be due to external contamination.

XPS and FT-IR results demonstrated successful incorporation of carboxyl and amine functionality on the surface of PAni:Ch nanocomposites after surface functionalization using glycine NHS ester. The mechanisms of surface functionalization have been discussed below with an insight into cell-biomaterial interactions.

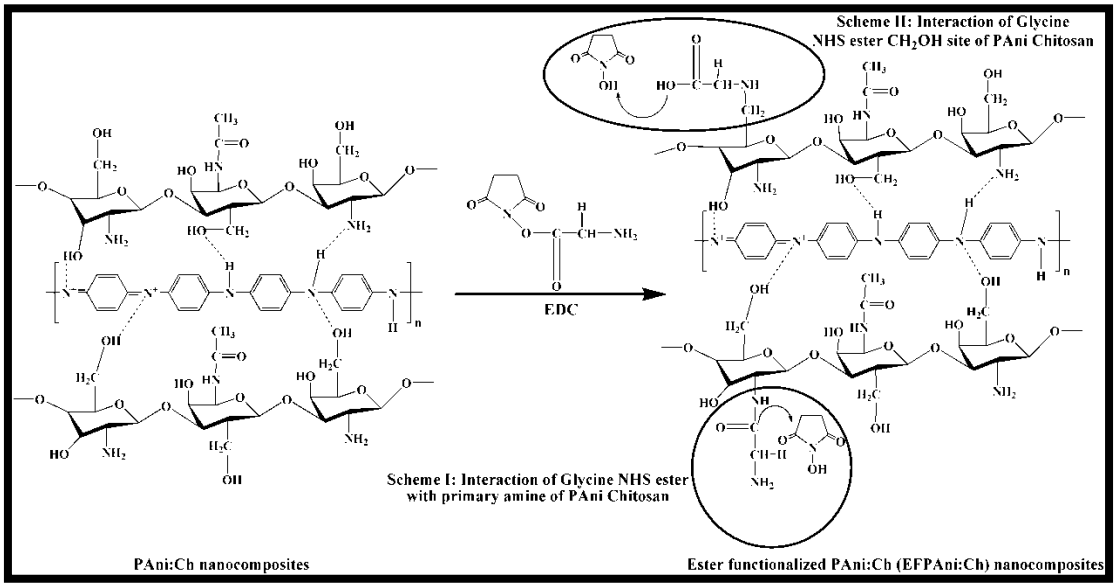

Figure 5.13. Probable interaction mechanisms of glycine NHS ester with PAni:Ch nanocomposites based on XPS and FTIR results.

It was previously shown that coupling of unprotected RGD peptides in water is possible, employing a two step procedure [401-403]. First, activation of the surface carboxyl group as an active ester that is less prone to hydrolysis is carried out, e.g.

NHS esters in EDC or DCC and subsequent coupling of peptide in water to the polymer surface via a stable covalent amide bond with the nucleophilic N-terminus of the peptide [401]. We have also followed the same concept in this work to functionalize the nanocomposite surface by unprotected glycine NHS ester but considering some possible side reactions with other reactive functionality present in the PAni:Ch nanocomposites surface.

XPS and FT-IR results demonstrated that there is no covalent interaction between PAni and Ch except weak electrostatic interactions and H-bonding between amine sites of PAni and hydroxyl groups and primary amine of Ch as shown in **Figure 5.13** (chemical structure of PAni:Ch nanocomposites), which is in agreement with previous reports [302]. The proposed chemical structure in **Figure 5.13** depicts the presence of hydroxyl and amine functionality on the nanocomposite surface, which is evident from XPS and FT-IR results. After surface modification of the nanocomposite surface by unprotected glycine NHS ester (BOC part removed), incorporation of glycine was confirmed from XPS and FT-IR results. XPS and FT-IR results suggest both carboxyl and amine functional groups on the surface of the nanocomposites after surface modification. The probable interaction mechanisms of unprotected glycine NHS ester with hydroxyl and amine functionality on the nanocomposite surface are shown in Scheme I and Scheme II of **Figure 5.13**. Usually, according to EDC-NHS chemistry; there is a higher probability of incorporation of glycine on to the nanocomposite surface via a stable amide bond formation between the primary amine group of Ch and the activated carboxyl group of glycine NHS ester giving an amine terminus surface as shown in Scheme I of **Figure 5.13**, which practically keeps the concentration of amine constant as also confirmed in the XPS results. The exceptional case here is the presence of free carboxyl groups on the modified nanocomposite surface, which is confirmed by both XPS and FT-IR results. Therefore, we have proposed coupling of the unprotected amine terminus of glycine (after removal of BOC) with the $–CH_2OH$ site, which is considered as an active site in Ch, giving a carboxyl terminus surface as depicted in Scheme II of **Figure 5.13**. This proposition is supported by previous reports, which suggest that the NHS-reactive ester intermediate is susceptible to nucleophilic attack by primary amines and carboxyl-terminus immobilization can also occur via carbodiimide-mediated chemistry [401].

5.2.7.3 Enhancement in wettability and surface energy after surface functionalization

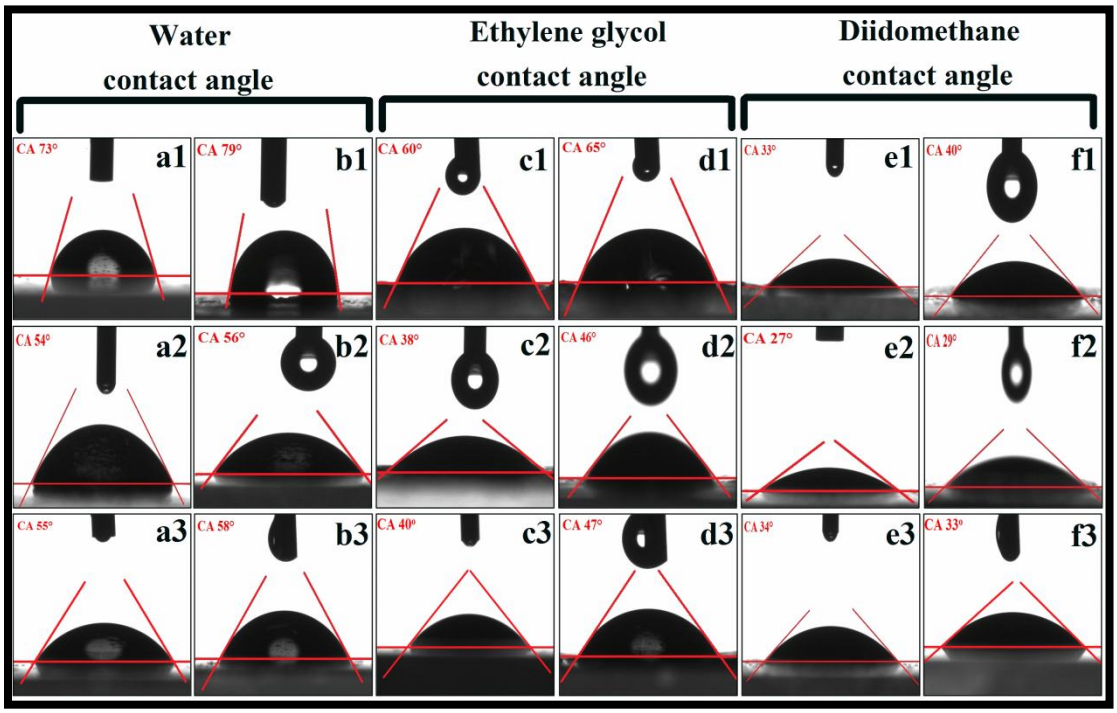

Figure 5.14. Representative contact angle images of using three probe liquids on PAni:Ch-4 wt% (a1:water; c1:ethylene glycol; e1:diiodomethane), PAni:Ch-6 wt% (b1:water; d1:ethylene glycol; f1:diiodomethane), GFPAni:Ch-4 wt% (a2:water; c2:ethylene glycol; e2:diiodomethane), GFPAni:Ch-6 wt% (b2:water; d2:ethylene glycol; f2:diiodomethane), EFPAni:Ch-4 wt% (a3:water; c3:ethylene glycol; e3:diiodomethane) and EFPAni:Ch-6 wt% (b3:water; d3:ethylene glycol; f3:diiodomethane).

Since the surface is the first point of contact between two materials, the surface and interfacial properties of materials play a crucial role in determining phenomena such as adhesion and adsorption. In this regard, surface properties of a material like wettability, hydrophilicity are important phenomenon for binding or adherence between two materials [404, 405]. Water contact angle is a characteristic parameter, which determines the interaction between a liquid and solid and represents the wettability of the material surface [366]. The surface wettability is closely related to the surface free energy and is governed by two factors: (i) chemical composition and

(ii) roughness of the surface [366]. Representative contact angle images on the non-functionalized and functionalized PAni:Ch nanocomposites films using two polar liquids: water and ethylene glycol and an apolar liquid diidomethane are shown in **Figure 5.14** and the average contact angle data are presented in **Table 5.9**.

Table 5.9. Average contact angle values for PAni:Ch nanocomposite films before and after surface modification (n = 3, mean ± SD).

Material	Water contact angle (°)	Ethylene glycol contact angle (°)	Diiodomethane contact angle (°)
PAni:Ch-4wt%	73.35±1.77	60.53±3.22	33.30±4.47
PAni:Ch-6wt%	79.50±2.18	65.19±2.01	40.50±3.54
GFPAni:Ch-4wt%	54.72±2.54	38.70±1.53	27.63±4.19
GFPAni:Ch-6wt%	56.57±3.65	46.52±1.12	29.87±3.80
EFPAni:Ch-4 wt%	55.43±1.65	40.81±1.91	34.55±4.15
EFPAni:Ch-6 wt%	58.68±2.44	47.10±3.15	33.71±3.87

Table 5.10. Surface energy and its components calculated by the OWRK method taking water and diiodomethane as probe liquids.

Material	OWRK method			
	γ_s^d mNm^{-1}	γ_s^p mNm^{-1}	γ_s mNm^{-1}	% Polarity
PAni:Ch-4wt%	42.72	5.36	48.08	11.14
PAni:Ch-6wt%	39.60	3.87	43.47	8.93
GFPAni:Ch-4wt%	45.60	13.36	58.96	22.66
GFPAni:Ch-6wt%	44.50	12.94	57.44	22.52
EFPAni:Ch-4 wt%	39.42	15.25	54.67	27.89
EFPAni:Ch-6 wt%	42.61	12.52	55.13	22.70

Table 5.11. Surface energy and its components calculated by AB method taking water, ethylene glycol and diiodomethane probe liquids.

Material	AB method					
	γ_s^{LW} mNm^{-1}	γ_s^- mNm^{-1}	γ_s^+ mNm^{-1}	γ_s^{AB} mNm^{-1}	γ_s mNm^{-1}	% Polarity
PAni:Ch-4wt%	42.60	17.48	0.92	7.93	50.53	15.69
PAni:Ch-6wt%	44.30	16.85	0.61	6.35	46.65	13.61
GFPAni:Ch-4wt%	43.08	35.76	1.10	12.54	55.62	22.54
GFPAni:Ch-6wt%	43.75	32.52	1.02	11.51	55.26	20.83
EFPAni:Ch-4 wt%	38.57	15.31	5.14	17.74	56.31	31.50
EFPAni:Ch-6 wt%	39.71	16.02	3.15	14.20	53.91	26.32

We have observed that non-functionalized nanocomposites with lower PAni content has lower water contact angle value, indicating greater wettability of the surface. This observation is slightly deviated from the Wenzel predication [366], which states that the wettability of a surface depends on the surface roughness and the contact angle at a surface is given as,

$$\cos\theta_a = r\cos\theta_o \qquad 5.2$$

where *r* is surface roughness factor and is defined as the ratio of rough surface area to total surface area, θ_a is the apparent contact angle measured at the geometric level of rough surface and θ_o is the contact angle on a smooth surface. Although, SEM shows increased surface roughness (*r*) with increase in PAni concentration in the nanocomposites, the water contact angle value for PAni:Ch-6 wt% (79°) is greater than that of PAni:Ch-4 wt% (73°). This suggest the chemical composition of the surface play the lead role, in this case, to determine the wettability of the surface, due to abundant amino and hydroxyl groups of Ch on the nanocomposites surface.

This proposition can be further correlated with much enhanced wettability of the glutaraldehyde and glycine NHS ester functionalized nanocomposites. **Table 5.9** shows a decrease in water contact angle up to 54° for GFPAni:Ch-4 wt%, 56° for GFPAni:Ch-6 wt%, 55° for EFPAni:Ch-4 wt% and 58° for EFPAni:Ch-6 wt% (after surface functionalization) from 73° for PAni:Ch-4 wt% and 79° for PAni:Ch-6

wt%(before surface functionalization), revealed the improved wettability of the material surface owing to incorporation of polar functionality such as aldehyde (glutaraldehyde functionalization) and carboxylic group (functionalization by glycine NHS ester). Usually, the high energy surfaces due to nature of the chemical bonds (viz. covalent, ionic) hold them together, possess higher wettability. Thus, the presence of chemical groups present on the surface of a material defines the wettability, which is one of the most prerequisite parameters correlated with cell-biomaterial interfacial interactions. Wettability of material surface can be evaluated by calculating surface energy of that material using contact angle values of different polar and apolar probe liquids on it. So far as, we have demonstrated directly the incorporation polar functional groups onto the surface of PAni:Ch nanocomposites with the help of FT-IR and XPS, there are no such direct method to calculate the total surface energy or surface tension except some indirect or semi-empirical methods.

In order to evaluate the difference in the surface wettability of the nanocompsites after surface functionalization, the Owens, Wendt, Rabel and Kaelble (OWRK) method has been used to determine the total surface energy (γ_s) and its polar (γ_s^p) and dispersive (γ_s^d)components [364-366]. It is a widely used method to determine the surface energy of polymeric materials and uses the contact angle data one polar liquid (water) and aploar liquid (diidomethane). The polar component of surface energy gives the estimation of concentration of polar groups that are present on the surface.The total surface energy (γ_s) along with its dispersive (γ_s^d) and polar (γ_s^p) components using two test liquids water/ethylene glycol and diiodomethane by OWRK method have been presented in **Table 5.10**. It has been observed that the total surface energy (γ_s) values of the glutaraldehyde functionalized nanocomposites and glycine NHS ester functionalized nanocomposites are greater than that of the non-functionalized nanocomposites [**Table 5.10**], which reveals enhancement in wettability of the functionalized surface. It has also demonstrated the enhancement in polar (γ_s^p) component of surface energy after surface functionalization, upto 13.36 mNm^{-1} (GFPAni:Ch-4 wt%), 12.94 mNm^{-1}(GFPAni:Ch-6 wt%), 15.25mNm^{-1} (EFPAni:Ch-4 wt%) and 12.52mNm^{-1} (EFPAni:Ch-6 wt%) from 5.36mNm^{-1}(PAni:Ch-4 wt%) and 3.87 mNm^{-1} (PAni:Ch-6 wt%) [**Table 5.10**]. Consequently, the percentages of surface polarity values of the functionalized nanocomposites are greater when compared to that of their non-functionalized counterparts [**Table 5.10**].

The observation suggest indirectly the incorporation of polar functional groups like hydroxyl, aldehyde functionalities after functionalization by glutaraldehyde and carboxyl, amine functionalities after functionalization by glycine NHS esteronto the surface of PAni:Ch nanocomposites. It is also to be noted that the presence of a small value of polar component of surface energy but not readily negligible, in case of non-functionalized nanocomposites can be assigned to the available already available hydroxyl and amino groups in Ch chains, which renders some surface wettability to the non-functionalized nanocomposites.

The Van Oss-Chaudhury-Good method, also known as the acid base (AB) method [364-366] was used to calculate the total surface energy and its components, which offers the advantage over others in the sense that it can provide a complete picture including the acidic and basic character of the surface beyond the total surface energy and dispersive and polar components. In this method, two polar liquids (water and ethylene glycol) and one apolar liquid (diiodomethane), were used as test liquids. The total surface energy and its components determined using the AB method are displayed in **Table 5.11**. In fact, the "polar" term designates three classes of compound viz. hydrogen bonding compounds, dipolar compounds and the compounds that interact with Lewis acids and bases [365, 366]. This AB method reported by Van Oss *et al*., distinguishes this acid base interaction as a component of surface energy denoted by γ^{AB}_{s}. As the OWRK method, the AB method also reveals enhancement in the total surface energy (γ_s) values of PAni:Ch nanocompositesafter surface functionalization by glutaraldehyde and glycine NHS ester [**Table 5.11]**.The most important observation is the remarkable enhancement in the acid-base γ^{AB}_{s} component of surface energy after surface modification which ultimately leads to improved hydrophilicity of the surface. It has been found that values of γ^{AB}_{s} are much greater for the functionalized nanocomposites than that of the non-functionalized nanocomposites [**Table 5.11**]. Although, surface polarity has been enhanced for both the glutaraldehyde functionalized and glycine NHS ester functionalized nanocomposites, the contribution of the each functionalization process towards the enhancement in the surface polarity can't be distinguished using OWRK method in the sense that nature of the incorporated functional groups i.e. acidic or basic. Interestingly, we have obtained significant results using AB method that can be

correlated well with the FT-IR and XPS results. For example, it is evident from the FT-IR and XPS results that functionalization by glutaraldehyde introduces mainly aldehyde functionality, which generally contributes towards the basic nature of the surface, whereas carboxyl functionality, introduced by functionalization with glycine NHS ester, contributes towards acidic character of the surface. The AB method gives this distinction, which the OWRK method could not. To speak more specifically, the Lewis acid (γ_s^+) components for EFPAni:Ch-4 wt% and EFPAni:Ch-6 wt% are enhanced upto 5.14mNm^{-1}and 3.15mNm^{-1}, respectively, from 0.92 mNm^{-1} (PAni:Ch-4 wt%)and 0.61 mNm^{-1} (PAni:Ch-6 wt%), which is due to incorporation of acidic carboxyl functionality [**Table 5.11**]. However, such enhancement in the Lewis acid (γ_s^+) components is not visible in case of glutaraldehyde functionalized surface, rather, it demonstrates significantly higher values of the Lewis basic (γ_s^-) components of GFPAni:Ch-4 wt% (35.76mNm^{-1}) and GFPAni:Ch-6 wt% (32.52mNm^{-1}) than that of non-functionalized PAni:Ch-4 wt% (17.48mNm^{-1})and PAni:Ch-6 wt% (16.85mNm^{-1}) owing to the incorporation of aldehyde functionality.

The enhancement in total surface energy value along with polar components, i.e., Lewis and acid and base component values after surface modification correlates with the improved cell-biomaterial interaction.

5.3 Biomedical applications of GFPAni:Ch nanocomposites

5.3.1 Enhanced urease activity and kinetics on GFPAni:Ch nanocomposites

5.3.1.1 Urease activity

The activity of both, immobilized and free, urease was determined using Nessler's method by measuring the amount of ammonia liberated in the urease-catalyzed reaction of hydrolysis of urea per unit time spectrophotometrically [406-408]. Urease catalyzes the hydrolysis of urea into carbon dioxide and ammonia as follows:

$$(NH_2)_2CO + H_2O \rightarrow CO_2 + 2NH_3$$

The produced ammonia reacts with Nessler's reagent to form a yellow colored product giving maximum absorbance at 470 nm:

$$2K_2HgI_4 + NH_3 + KOH \rightarrow HgO.Hg(NH_3)I \downarrow + 2H_2O$$

Nessler's reagent Yellow color

Briefly, the activity of free urease and immobilized urease was determined using the following formula:

$$Urease\ activity\left(\frac{\mu mol.min^{-1}}{mg}\right) = \frac{OD_{sample} - OD_{PBS}}{Slope \times t \times Protein\ content\ in\ mg} \times n \quad 5.3$$

Here, OD_{sample} and OD_{PBS} are the measured absorbance values of sample and enzyme buffer, respectively, t is the incubation time and n is the dilution factor. The protein content is determined by measuring the difference in weight of the substrate (Dimension: 1 cm×1 cm) before and after immobilization of urease (Concentration: 1 mg/mL). The slope is determined from the calibration curve as shown in **Figure 5.16**.

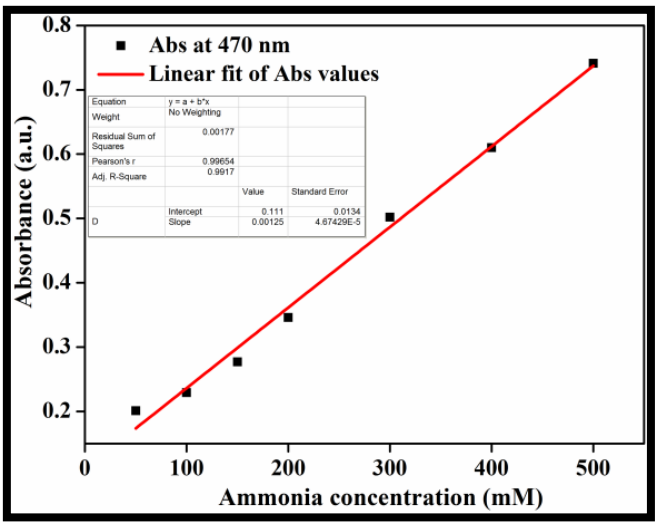

Figure 5.15. Calibration curve to determine the slope. Slope is 0.00125 mM^{-1} i.e., 3.0 × 10^{-3} μmol^{-1} (Since the total volume of the solution is 2 mL).

Figure 5.16 (a) depicts the variation of activity of free urease and immobilized urease on non-functionalized nanocomposites (PAni:Ch-4 wt% and PAni:Ch-6 wt%) and glutaraldehyde functionalized nanocomposites (GFPAni:Ch-4 wt% and GFPAni:ch-6 wt%), with time. Urease, immobilized on the glutaraldehyde functionalized nanocomposites, shows enhanced activity as compared to the urease activity, immobilized on the non-functionalized nanocomposites. The free urease shows maximum activity of 32.42 ± 2.2 $\mu mol.min^{-1}.mg^{-1}$ at t = 15 min, while PAni:Ch-4 wt%, PAni:Ch-6 wt% and GFPAni:Ch-4 wt% and GFPAni:Ch-6 wt% demonstrate

urease activity of 23.45 ± 1.78, 21.75 ± 2.78, 30.23 ± 3.54 and 30.12 ± 1.98 μmol.min^{-1}.mg^{-1}.cm^{-2}, respectively, at t = 15 min. This means PAni:Ch-4 wt%, PAni:Ch-6 wt% and GFPAni:Ch-4 wt% and GFPAni:Ch-6 wt% retained maximum of 73% ± 3.32, 67% ± 4.71, 95% ± 6.45 and 94% ± 3.52 urease activity of free urease activity.

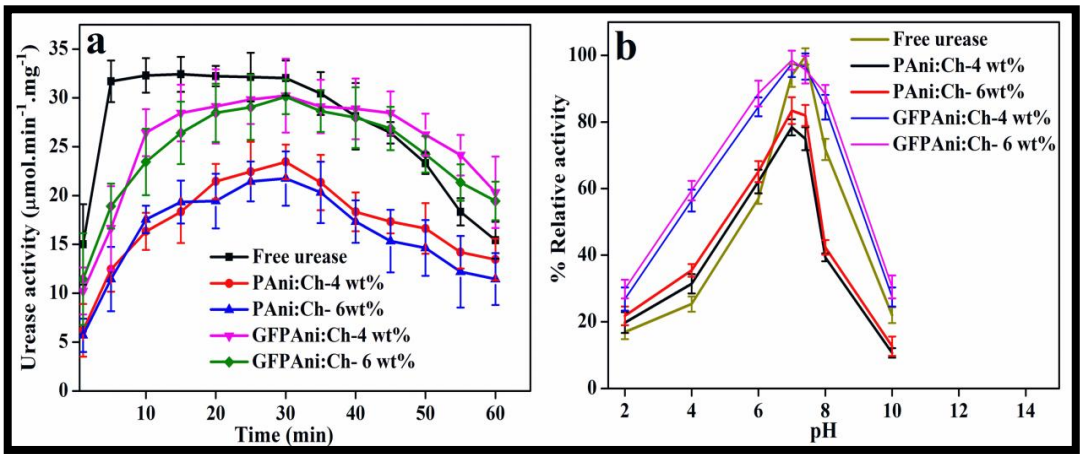

Figure 5.16. (a) Activity of free urease and immoblized urease on non-functionalized and glutaraldehyde functionalized PAni:Ch nanocomposites at room temperature (p^H = 7.4). (b) pH stability of the activity of free urease and immoblized urease on non-functionalized and glutaraldehyde functionalized PAni:Ch nanocomposites.

One-way ANOVA analysis reveals that the urease activity on GFPAni:Ch-4 wt% and GFPAni:Ch-6 wt% is statistically different at $p<0.01$ from that on the non-functionalized PAni:Ch-4 wt% and PAni:Ch-6 wt%. However, at t = 15 min, the urease activity on GFPAni:Ch-4 wt% and GFPAni:Ch-6 wt% is not significantly different from the free urease activity. There are also no significant different in urease activity on GFPAni:Ch-4 wt% and GFPAni:Ch-6 wt%. The activity of urease immobilized on functionalized nanocomposites represents an improvement in the previously reported immobilized urease activity of 51%, 20-30%, 73% and 80% [407]. Interestingly, after 60 min, the urease immobilized on the functionalized nanocomposites retain enhanced activity of 20.34 ± 3.66 μmol.min^{-1}.mg^{-1}.cm^{-2} (GFPAni:Ch-4 wt%) and 19.45 ± 2.03μmol.min^{-1}.mg^{-1}.cm^{-2} (GFPAni:Ch-6 wt%), when compared to free urease activity of 15.43 ± 1.96 μmol.min^{-1}.mg^{-1}. The improved urease activity on the functionalized nanocomposites is attributed to the improved surface hydrophilicity of the nanocomposites after surface functionalization by

glutaraldehyde. The incorporated aldehyde functionality on the surface of the nanocomposites offers covalent binding with the immobilized urease as it is believed that due to its higher activity of glutaraldehyde towards amino groups, aldehyde functionality on the nanocomposites will form covalent bond the amino groups of urease. Moreover, amino groups already present in Ch may also interact with the carboxylic group of urease covalently, which may also contribute towards the improved activity of the immobilized urease. This is the reason why the non-functionalized nanocomposites demonstrate more than 65% activity of the free urease activity. The results further demonstrate that there is no effect of surface roughness on the immobilization efficiency or urease activity as nanocomposites with more rough surface with higher PAni content [as revealed by SEM in **Figure 5.1(d)**] has slightly lower urease activity as compared to that of nanocomposites with lower PAni content.

It is well known that the pH activity of immobilized urease depends on the substrate chosen. **Figure 5.16 (b)** displays the pH stability of the activity of free urease and immobilized urease on different non-functionalized and functionalized PAni:Ch nanocomposites. The reactions were carried out at different pH values (2-10) by the addition of suitable buffers. Both free and immobilized urease demonstrate maximum activity at pH=7.4, however, the immobilized urease on the functionalized nanocomposites maintains higher relative activity than that of free urease and immobilized urease on non-functionalized nanocomposites. This indicates the immobilized urease on the functionalized nanocomposites is less sensitive to the change in pH level. This may attributed to the presence of different functionalities such as aldehyde, amino, hydroxyl groups on the surface of the glutaraldehyde functionalized nanocomposites.

There are several possibilities for lowering of the free urease activity after a certain time. In our case, we have observed that free urease activity drops after 40 mins, when compared to the activity of the immobilized urease [**Figure 5.16 (a)**]. In fact, it starts to drop after 10 min, if we notice carefully. It indicates that the rapid catalysis of the enzyme, suggesting easy access of substrate (urea) to the catalytic sites of the enzyme. There is less possibility of adsorption of the enzyme to be adsorbed on the flat walls the of glass vial used for the experimentation. So, as soon as the enzyme is added to the substrate, the whole enzyme is being exposed to substrate and eventually, due to no diffusional resistance, all the enzyme molecules catalyze the substrate at a time, which is evident from the highest activity of the free

urease after 5 min [**Figure 5.16 (a)**]. Even when the enzyme is physically adsorbed on the walls of the vials, it is still easily accessible to the substrate for catalysis. Therefore, a common reason for this slowing down of the speed (rate) of the reaction is that the substrate within the mixture is being used up and thus becoming limiting []. In the contrary, the immobilized urease encounters diffusional resistance on account of their tight binding with the scaffolds and the immobilized urease reaches slowly to the substrates due to its higher stability. There are also several reasons of lowering free enzyme activity over time such as conformation changes of the enzymes causing its denaturation when it is adsorbed on the walls of the vial, change in pH over time, etc.

5.3.1.2 Reusability

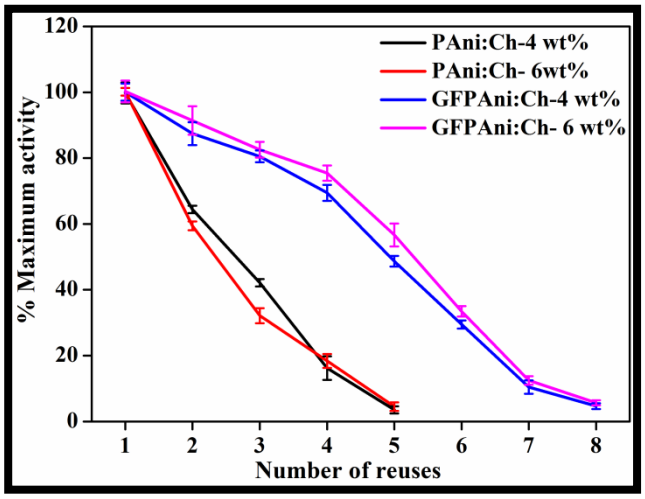

Figure 5.17. Reusability of urease immobilized non-functionalized and glutaraldehyde functionalized PAni:Ch nanocomposites at room temperature (pH=7.4).

Figure 5.17 shows the stability of immobilized urease on the non-functionalized and functionalized PAni:Ch nanocomposites stored at 4°C and the reaction was performed at room temperature. The results reveal that urease immobilized on GFPAni:Ch-4 wt% and GFPAni:Ch-6 wt% retains 10.50% and 9.43% of the initial activity, after 8 uses, while the urease immobilized is able to retain only 5.01% (PAni:Ch-4 wt%) and 4.98% (PAni:Ch-6 wt%) of the initial activity after 5 uses. The improved reusability of the urease immobilized on the glutaraldehyde functionalized nanocomposites is

assigned to the tight binding between the substrate and the enzyme through covalent bond [407].

5.3.1.3 Kinetics of immobilized urease

The kinetics of free urease and immobilized urease are presented in **Figure 5.18** by plotting 1/Urea concentration in the X-axis and inverse of their corresponding rate of reaction in the Y-axis, which is known as Lineweaver-Burk plot. The linearity of the Lineweaver-Burk plots suggest both free and immobilized urease follow Michaelis-Menten kinetics following the equation [406, 408]:

$$\frac{1}{V} = \frac{K_m}{V_{max}}\frac{1}{[S]} + \frac{1}{V_{max}} \qquad 5.4$$

Here, where V and V_{max} are actual and maximum reactions rates, respectively, K_m is the Michaelis constant and [S] is substrate concentration.

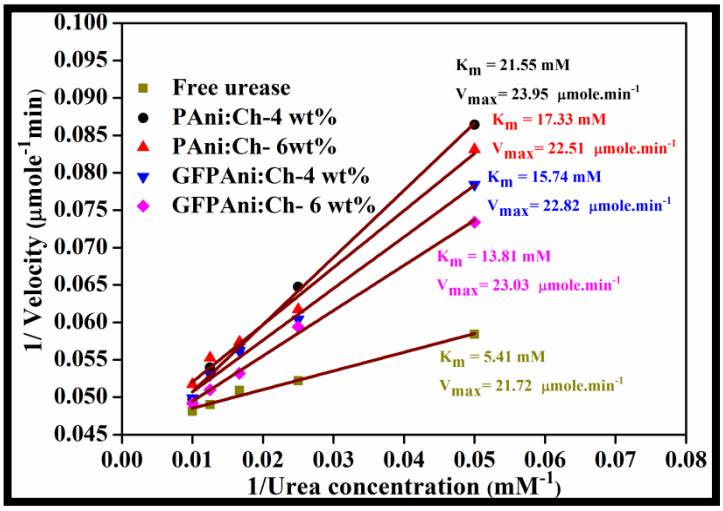

Figure 5.18. Lineweaver-Burk plots of free urease, immobilized urease on non-functionalized and glutaraldehyde functionalized PAni:Ch nanocomposites. Reactions were carried out in PBS (pH=7.4) at room temperature.

For low concentrations of substrate the reaction is of the first order, for high concentrations it changes into zero order when the reaction rate is independent of substrate concentration. This range of concentration was used for enzyme activity determinations. The calculated values of the kinetic parameters: the Michaelis constants (K_m) and the maximum reaction rates (V_{max}) are shown in **Figure 5.18**. It

has been found that K_m values of immobilized urease on GFPAni:Ch-4 wt% (13.81 ± 2.56 mM) and GFPAni:Ch-6 wt% (15.74 ± 1.87 mM) are greater than that of free urease (5.41 ± 1.26 mM). However, the K_m values for immobilized urease on the non-functionalized nanocomposites (17.33 ± 4.36 and 21.55 ± 2.24 mM for PAni:Ch-4 wt% and PAni:Ch-6 wt%, respectively) is higher than that of functionalized nanocomposites indicating the tighter binding between the functionalized nanocomposites and the enzyme than that of the non-functionalized nanocomposites owing to their improved surface polarity or hydrophilicity. One-way ANOVA analysis demonstrates that the K_m and V_{max} values of the immobilized urease on the functionalized nanocomposites are statistically different than those of the immobilized urease on the non-functionalized nanocomposites at $p<0.01$. The K_m and V_{max} values of the free urease are significantly different at $p<0.01$ than those for all the immobilized urease. The increase in Michaelis menten constant K_m value is a consequence of the conformational changes in the enzyme as a result of formed enzyme-substrate complex and more difficulty in accessibility of the substrate by the immobilized enzyme to its active sites/increased diffusional resistance encountered by the substrate in its approach to the catalytic sites and by the reaction product leaving from the same place. It may also arise from the confinement of enzyme molecules within the nanocomposite matrices during the process of immobilization. However, the maximum rate of reaction catalyzed by the immobilized urease is slightly higher than that of the free urease.

5.3.2 Biocompatible GFPAni:Ch nanocomposites for enhanced MDA-MB-231 cell adhesion and proliferation

5.3.2.1 Hemolysis activity

Hemocompatibility, also known as blood compatibility, is an important property of biomaterials, which strongly depends on the materials chosen. Therefore, materials intended for biomedical applications involving direct contact with living tissues, are to be checked for its blood compatibility. Hemolysis is the rupturing of RBCs or erythrocytes and thereby, releases the cytoplasmic materials, mainly hemoglobin from within the red blood cells into the blood plasma. Thus, the materials, which cause damage of host cytoplasmic membrane of RBCs and cell lysis and death, are known

as hemolysins. The hemocompatibility of the non-functionalized and functionalized PAni:Ch nanocomposites has been tested in terms of their hemolysis activity with mammalian red bold cells (RBCs) and the results are presented in **Figure 5.19**.

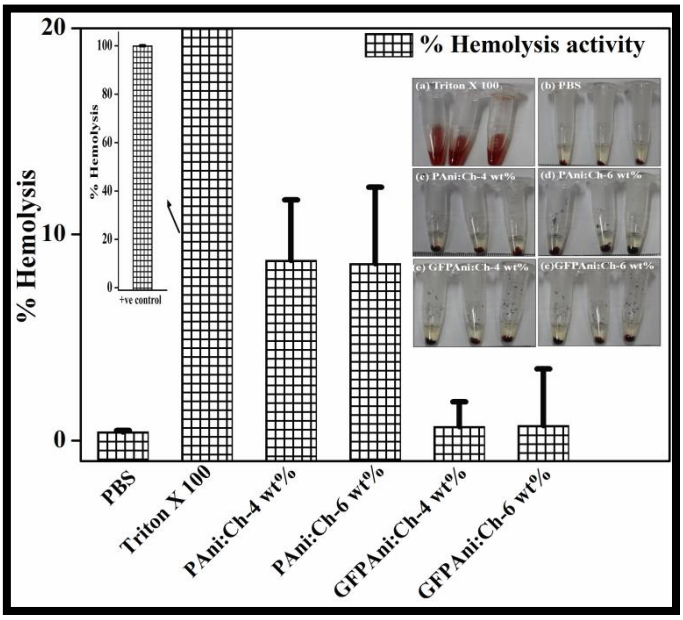

Figure 5.19. Percentage hemolysis (Mean ± S.D, n=4) shown by the non-functionalized and functionalized PAni:Ch nanocomposites as compared to negative control (Phosphate buffer saline, pH= 7.4) and positive control (Triton X 100). Inset shows photographs of RBC treatment with different materials as labeled.

Here, Triton X-100 has been used as positive control, which induces 100% hemolysis and phosphate buffer saline (PBS, pH=7.4) has been used as negative control, which causes no damage to RBCs. For hemolysis activity measurement, 5 mg of each nanocomposites film has been treated with RBCs and the respective photographs are shown in the inset of **Figure 5.19**. According to the ASTM F 756-00 standard, all materials can be categorized on the basis of their hemolysis activity as follows [409, 410]:

% Hemolysis < 2: non-hemolytic

2 < % Hemolysis <5: slightly hemolytic

% Hemolysis > 5: hemolytic

The glutaraldehyde functionalized nanocomposites, i.e., GFPAni:Ch-4 wt% and GFPAni:Ch-6 wt% demonstrate very less hemolysis activity of 0.86% ± 1.02 and 0.92% ± 1.52, which is nearly equal to the hemolysis activity exhibited by the negative control (0.41% ± 0.07), indicating non-hemolytic nature of the nanocomposites. On the other hand, the non-functionalized nanocomposites, i.e.,PAni:Ch-4 wt% and PAni:Ch-6 wt% demonstrate hemolysis activity more than 5% suggesting hemolytic nature of the nanocomposites. The lower hemolysis activity of the functionalized nanocomposites is attributed to the improved surface hydrophilicity and softer nature [lower stiffness constant as discussed in **Section 5.2.4**] of the nanocomposites after functionalization of glutaraldehyde, whereas the surface roughness, the electrostatic interaction with cell surface and the rigid nature [higher stiffness constant as discussed in **Section 5.2.4**] of the non-functionalized nanocomposites contribute towards their hemolytic behaviour. The results suggest improved biocompatibility of the PAni:Ch nanocomposites after surface functionalization by glutaraldehyde and thereby, gives the initial indication of their potential in biomedical applications involving direct contact with living tissues.

5.3.2.2 MTS proliferation assay

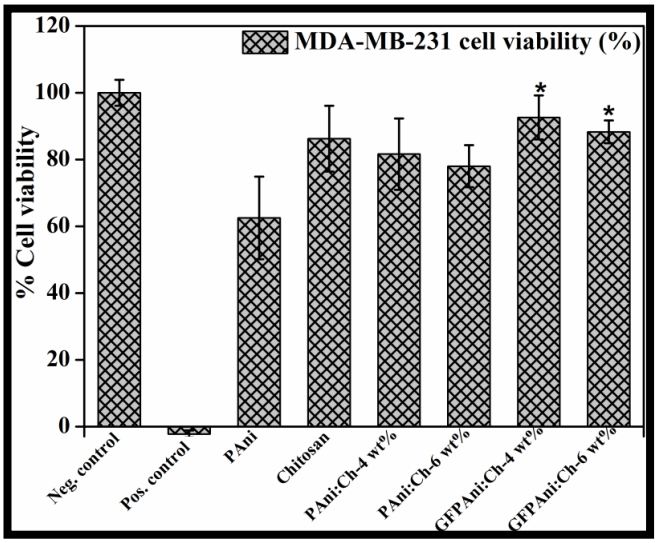

Figure 5.20. Percentage of MDA-MB-231 cell viability on the non-functionalized and glutaraldehyde functionalized PAni:Ch nanocomposites in direct contact after 24 h of culture as compared to tissue culture plastic (TCP) as a negative control and *tert* butyl maleate as a positive control. Data were Mean ± S.D, n=3. $^{*}\leq 0.05$.

To evaluate the biocompatibility of the non-functionalized and glutaraldehyde functionalized nanocomposites, MDA-MB-231 cell viability was measured in direct contact with the different nanocomposites films after 24 h of culture. This has been performed by MTS cell proliferation assay, where the metabolically active cells reduce the tetrazolium compound (MTS) into a water soluble formazan product and the non-viable cells rapidly lose their ability to do that. The colored formazan product gives absorption maximum at 490 nm and the production of the colored formazan product is proportional to the number of viable cells [320]. The negative control is believed to induce maximum cell viability, whereas the positive control (*tert* butyl maleate) causes maximum cell death. The percentage of MDA-MB-231 cell viability on different nanocomposites films are shown in **Figure 5.20** along with raw PAni nanofibers and Ch. The MTS results with MDA-MB-231 cells indicates significantly better cell viability and proliferation on glutaraldehyde functionalized nanocomposites than that on the non-functionalized nanocomposites and raw PAni nanofibers, at $p<0.05$ ($p=0.0046$). However, non-functionalized nanocomposites and pure Ch have been also found to be biocompatible as they support approximately 80% cell viability [411]. It was also noted that nanocomposites with lower PAni content, i.e., 4 wt% nanocomposites (both non-functionalized & functionalized) show slightly better cell viability than that of nanocomposites with 6 wt% PAni content (both non-functionalized & functionalized). Overall, the significant improvement in cell viability on glutaraldehyde functionalized nanocomposites supports the hypothesis that enhanced surface hydrophilicity conferred onto the surface of the nanocomposites significantly increases adhesive, metabolising cell fraction.

5.3.2.3 Acridine orange/ethidium bromide (AO/EtBr) staining

To visualize the MDA-MB-231 cells cultured on different PAni:Ch nanocomposites, the cells were stained with acridine orange (AO) and ethidium bromide (EtBr) for nucleic acid staining after 48 h of culture following the procedure as discussed in **Chapter III**. The fluorescence micrographs of AO/EtBr stained MDA-MB-231 cells on the non-functionalized and glutaraldehyde functionalized nanocomposites films after 48 h of culture are shown in **Figure 5.21**.

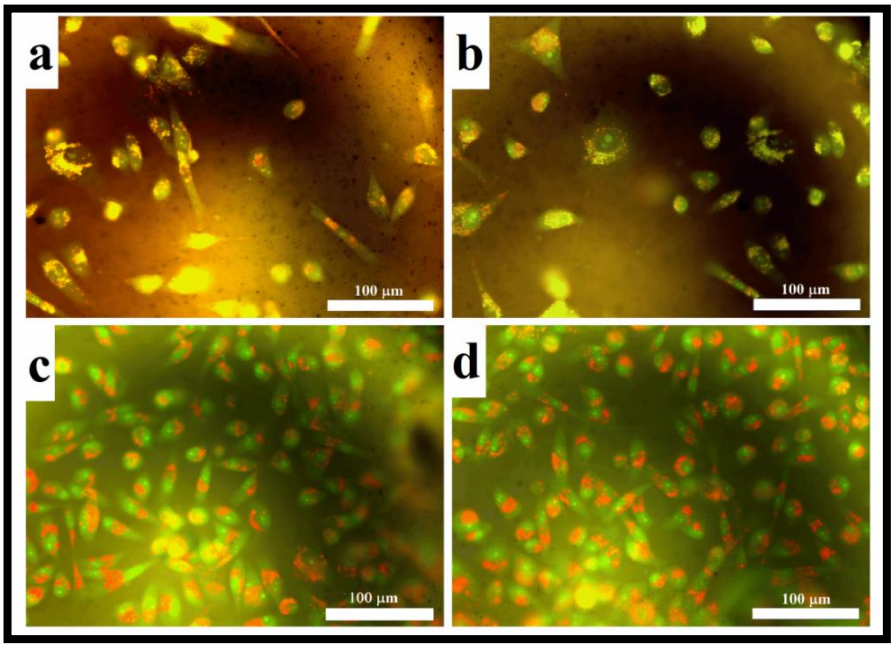

Figure 5.21. Fluorescence micrographs of AO/EtBr stained MDA-MB-231 cells on (a) PAni:Ch-4 wt%, (b) PAni:Ch-6 wt%, (c) GFPAni:Ch-4 wt% and (d) GFPAni:Ch-6 wt% after 48 h of culture.

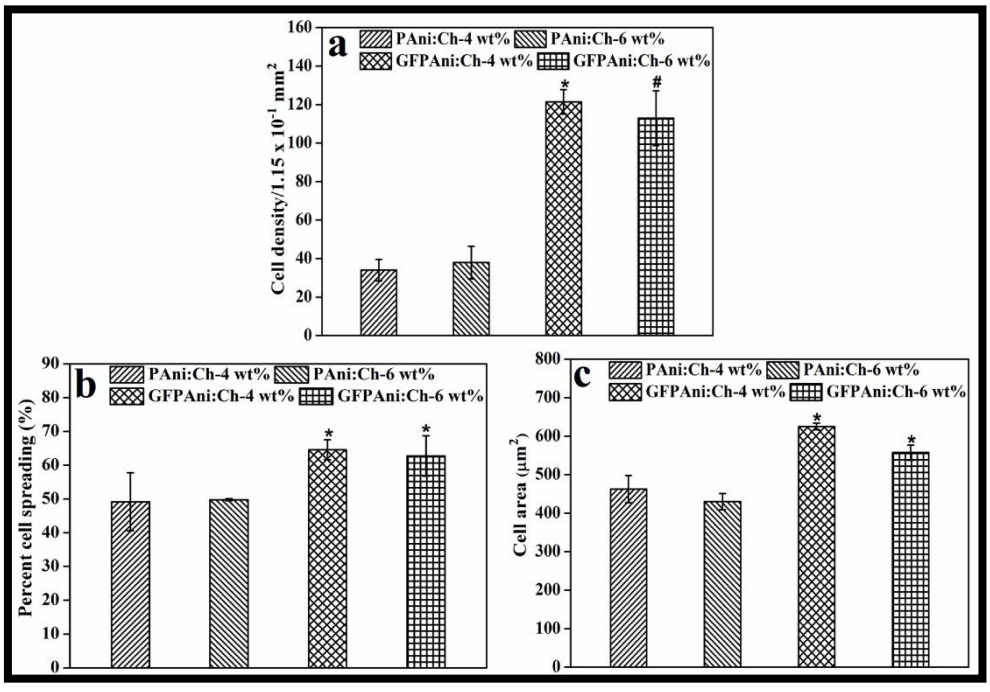

Figure 5.22. Quantitative analysis of (a) cell counts, (b) percentage of cell spreading and (c) area per cell on non-functionalized and functionalized PAni:Ch nanocomposites after 48 h of culture. Data were Mean ± S.D., n=3.$^{\#}$ and * indicate the statistical significance at $p \leq 0.01$ and $p \leq 0.05$, respectively.

The staining can be visualized throughout the whole body of the MDA-MB-231 cells. It has been observed that the cells cultured on glutaraldehyde functionalized nanocomposites, i.e., GFPAni:Ch-4 wt% and GFPAni:Ch-6 wt% [**Figure 5.21 (c) & (d)**] possess elongated or polygonal morphology with higher cell counts, indicating healthier morphology than that of cultured on the non-functionalized nanocomposites, i.e., PAni:Ch-4 wt% and PAni:Ch-6 wt%. The cells cultured on the non-functionalized nanocomposites possess round morphology with irregular shapes [**Figure 5.21 (a) & (b)**].

The density and cellular activities, i.e., cell morphology and spreading, of MDA-MB-231 cells on different PAni:Ch nanocomposites after 48 h of culture, have been quantified by processing the respective fluorescence micrographs of acridine orange stained cells in ImageJ software. The quantitative analysis results are presented in **Figure 5.22**. The cell density on the functionalized nanocomposites, i.e. GFPAni:Ch-4 wt% (121±6) and GFPAni:Ch-6 wt% (114±14) is significantly higher than that of the non-functionalized nanocomposites, i.e. PAni:Ch-4 wt% (34±6)and PAni:Ch-6 wt% (38±9) [**Figure 5.22 (a)**]. The difference in the cell density on GFPAni:Ch-4 wt% and PAni:Ch-4 wt% is statistically significant at $p \leq 0.05$ ($p=0.007$), whereas the cell density on GFPAni:Ch-6 wt% and PAni:Ch-6 wt% is statistically different at $p \leq 0.01$ ($p=0.0025$). The percentage of cell spreading on GFPAni:Ch-4 wt% (66%±5) and GFPAni:Ch-6 wt% (62%±6) is also significantly higher than that of the PAni:Ch-4 wt% (49%±9) and PAni:Ch-6 wt% (50%±3) at$p \leq 0.05$ [**Figure 5.22 (b)**]. Each MDA-MB-231 cell cultured on GFPAni:Ch-4 wt% and GFPAni:Ch-6 wt% possess an area of projection of 625 μm^2 ±9 and 557 μm^2 ±20, which is greater than the area of projections of each cell cultured on the non-functionalized nanocomposites and statistically different at $p \leq 0.05$ [**Figure 5.22 (c)**].
The results suggest that glutaraldehyde functionalized nanocomposites offer themselves as suitable biomaterial scaffold for better cell morphology, enhanced cell density and spreading owing to their enhanced surface properties such as polar functionality, hydrophilicity, wettability and surface energy.

5.3.2.4 Cell attachment

To confirm the cell attachment, SEM of the MDA-MB-231 cells cultured on the different PAni:Ch nanocomposites after 48 h, were performed and the results are shown in **Figure 5.23**. The MDA-MB-231 cells adhere, spread well and adopt

elongated or polygonal morphology on the glutaraldehyde functionalized PAni:Ch nanocomposites [**Figure 5.23 (c) & (d)**] as compared to the round and irregular shapes of cells on the non-functionalized nanocomposites [**Figure 5.23 (a) & (b)**]. Thereby, SEM confirms the observation obtained by AO/EtBr staining. The enhanced cellular activities on the glutaraldehyde functionalized nanocomposites indicate the potential of these materials in tissue engineering applications.

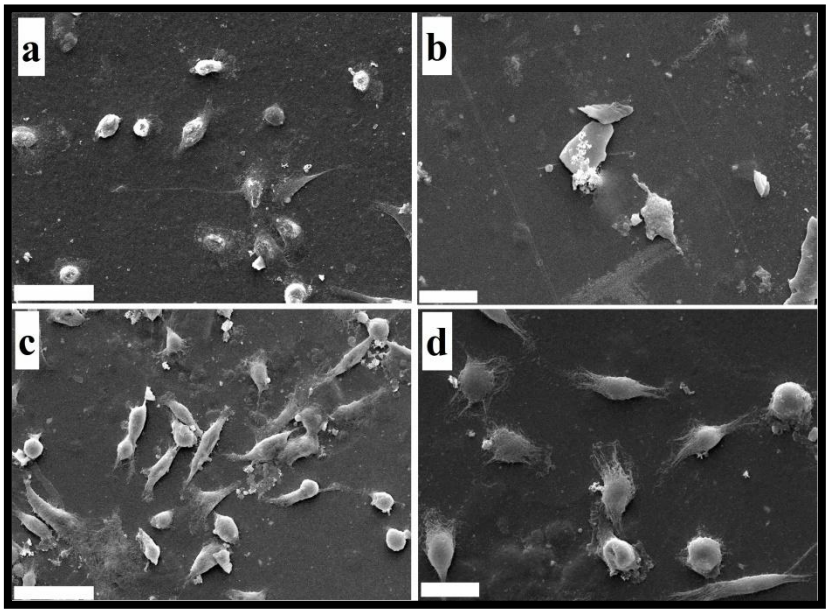

Figure 5.23. Scanning electron micrograph of MDA-MB-231 cells cultured on (a) PAni:Ch-4 wt% (Scale bar = 50 μm), (b) PAni:Ch-6 wt% (Scale bar = 20 μm), (c) GFPAni:Ch-4 wt% (Scale bar = 50 μm) and (d) GFPAni:Ch-6 wt% (Scale bar = 20 μm) after 48 h.

5.4 Biomedical applications of EFPAni:Ch nanocomposites

5.4.1 Biocompatible EFPAni:Ch nanocomposites for enhanced 3T3 fibroblast adhesion and proliferation

5.4.1.1 Hemolysis activity

The hemolysis activity of the glycine NHS ester functionalized PAni:Ch nanocomposites were checked as discussed in **Section 5.4.2.1**.**Figure 5.24** shows that very less hemolytic activity of glycine NHS ester functionalized PAni:Ch nanocomposites, i.e., EFPAni:Ch-4 wt% (0.66% ± 0.20) and EFPAni:Ch-6 wt%

(0.72% ± 0.15), which is comparable to non-hemolytic control PBS (0.41% ± 0.07), while the non-functionalized nanocomposites, i.e., PAni:Ch-4 wt% and PAni:Ch-6 wt% are hemolytic with percent hemolysis of 8.73% ± 2.64 and 8.57% ± 3.51, respectively as discussed in **Section 5.4.2.1**. The enhanced surface hydrophilicity due to incorporation of polar functionalities such as carboxyl and amino groups and softer nature of the nanocomposites after surface functionalization (lower stiffness constant) contribute towards the lower hemolysis activity of the glycine NHS ester functionalized PAni:Ch nanocomposites, indicating their improved blood compatibility [412].

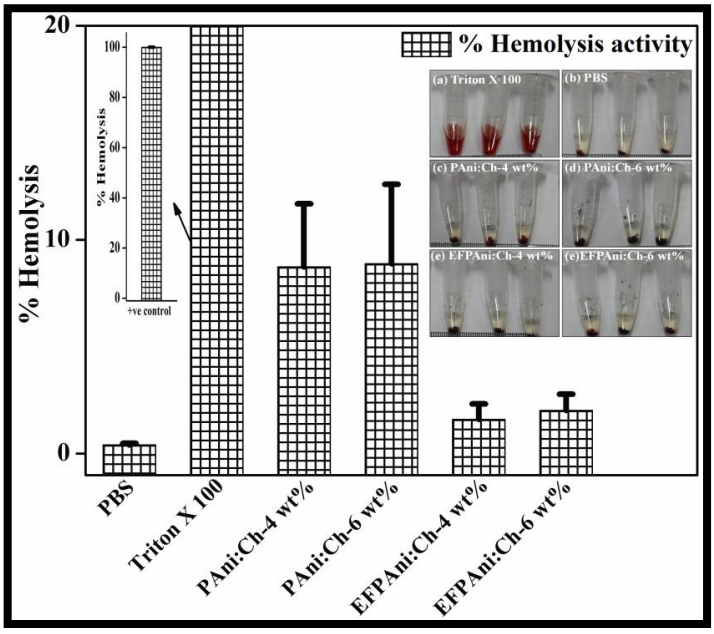

Figure 5.24. Percentage hemolysis (n = 4, mean ± S.D) shown by the non-functionalized and glycine NHS ester functionalized PAni:Ch nanocomposites as compared to negative control (Phosphate buffer saline, pH = 7.4) and positive control (Triton X 100). Inset shows photographs of RBC treatment with different materials as labeled.

5.4.1.2 MTS proliferation assay

The MTS proliferation assay has been performed following the same procedure as discussed in **Chapter III** with two cell lines: 3T3 fibroblasts and neuronal model rat pheocytochroma PC12 to evaluate the biocompatibility of the glycine NHS ester functionalized PAni:Ch nanocomposites. **Figure 5.25** shows percent cell viability on

different materials. Tissue culture plastic (TCP) was used as a negative control with maximum cell adhesion, whilst cytotoxic polymer (tributyltin maleate) was used as a positive control with no MTS signal. The MTS results with 3T3 fibroblasts and PC12 cells confirm that significantly better cell viability and proliferation on glycine NHS ester functionalized PAni:Ch nanocomposites than on the non-functionalized nanocomposites, at $p<0.05$. However, the non-functionalized nanocomposites are also found to be biocompatible as they support approximately 80% cell viability [411]. It was also noted that nanocomposites with lower PAni content, i.e., 4 wt% nanocomposites (both non-functionalized & functionalized) show slightly better cell viability than 6 wt% nanocomposites (both non-functionalized & functionalized), at $p<0.05$. Overall, the significant improvement in cell viability on glycine NHS ester functionalized supports the hypothesis that amine and carboxyl functionality incorporated onto the surface of the nanocomposites significantly increases adhesive, metabolising cell fraction.

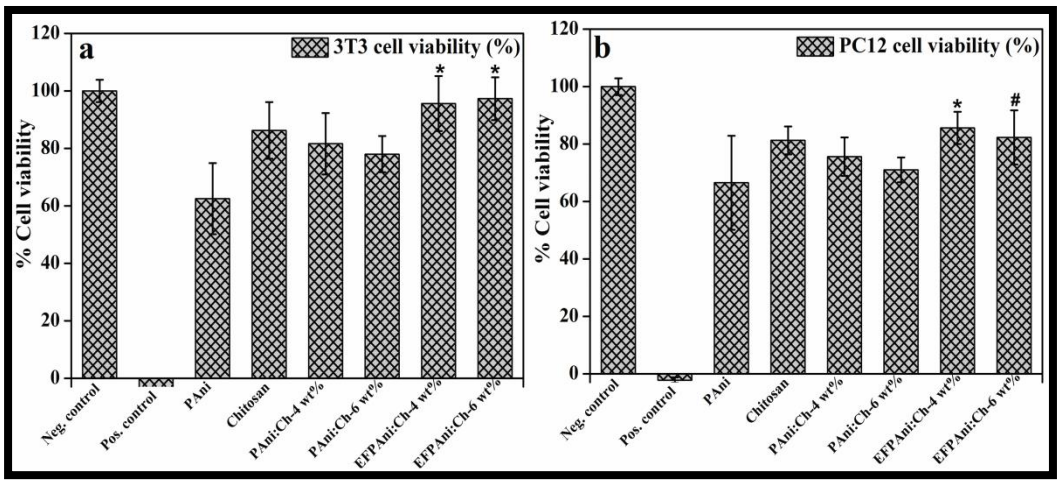

Figure 5.25. Percentage cell viability after 24 h of culture on glycine NHS ester functionalizednanocomposites compared to non-functionalized nanocomposites, raw materials (n = 4, mean ± SD) with (a) 3T3 fibroblasts and (b) PC12 cells. *Significant differences between negative control and test materials at p<0.05; #Significant differences between unmodified nanocomposites and modified nanocomposites at p<0.05.

5.4.1.3 Improved 3T3 fibroblast adhesion and morphology

5.4.1.3.1 Live/dead assay

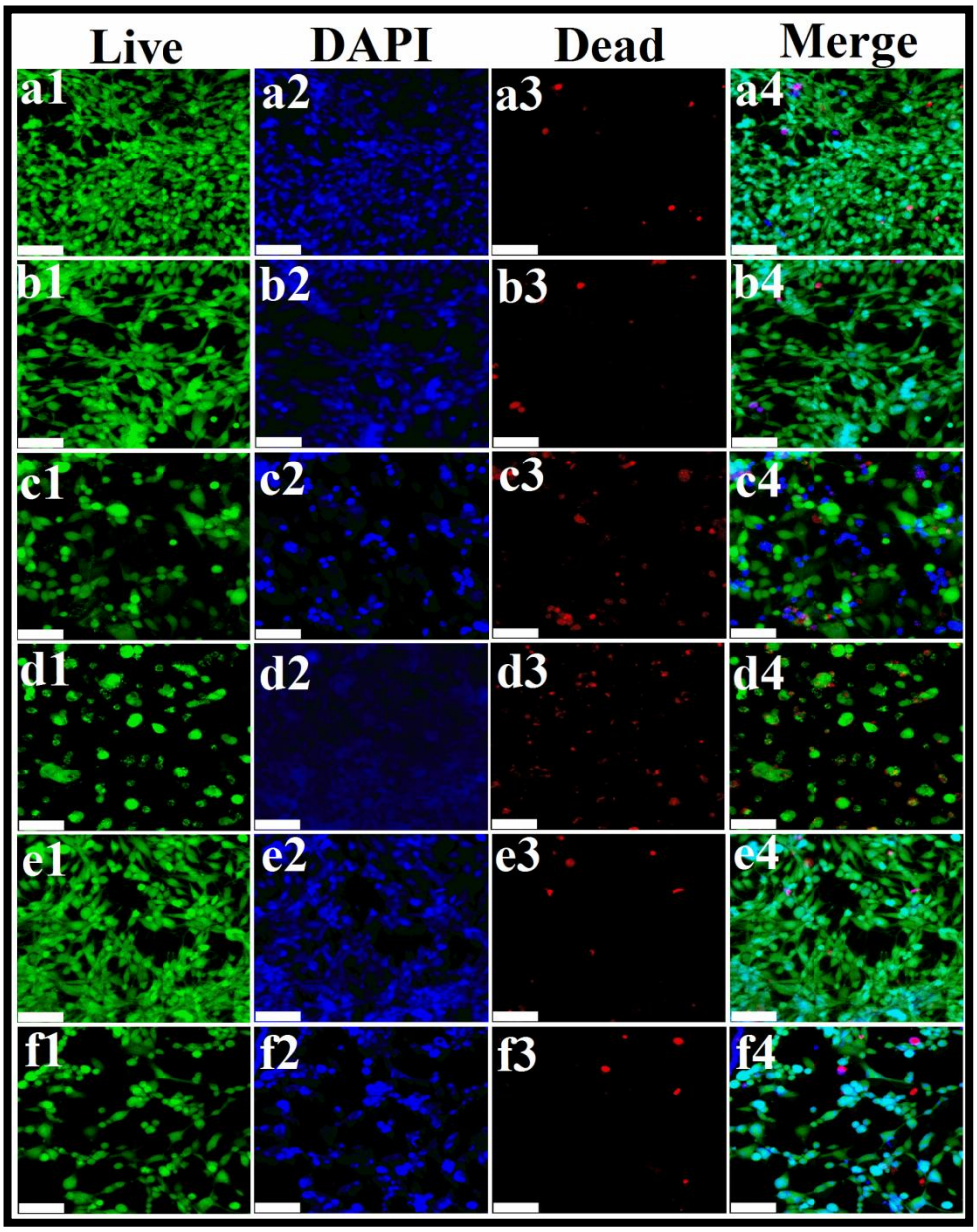

Figure 5.26. Confocal images of 3T3 fibroblasts after 24 h of culture on pure tissue culture plastic (a1-a4), Ch (b1-b4), PAni:Ch-4 wt% (c1-c2), PAni:Ch-6 wt% (d1-d4), EFPAni:Ch-4 wt% (e1-e4) and EFPAni:Ch-6 wt% (f1-f4) in direct contact by live/dead staining using EthD-1 (staining dead cells), calcein AM (staining live cells) and DAPI (staining nucleic acid). Live cells were stained with green, dead cells were stained with red, and nucleic acids were stained with blue. (Scale bar = 75 μm).

The live/dead assay was performed to confirm the MTS results and to visualize the live and dead cells. The confocal images of 3T3 fibroblasts after 24 h of culture on different scaffolds are shown in **Figure 5.26**. It has been observed that the cell spreading process was initiated on the EFPAni:Ch-4 wt% [**Figure 5.26 (e1-e4)**]and EFPAni:Ch-6 wt% [**Figure 5.26 (f1-f4)**] along with some round shaped and elongated cells, which had a healthier morphology than those grown on the PAni:Ch-4 wt% [**Figure 5.26 (c1-c4)**]and PAni:Ch-6 wt% [**Figure 5.26 (d1-d4)**]. Moreover, the number of dead cells (EthD-1 stained red) appears to be higher on the non-functionalized nanocomposites, i.e. PAni:Ch-4 wt% [**Figure 5.26 (c3)**] and PAni:Ch-6 wt% [**Figure 5.26 (d3)**] than those grown on the functionalized nanocomposites, i.e., EFPAni:Ch-4 wt% [**Figure 5.26 (e3)**] and EFPAni:Ch-6 wt% [**Figure 5.26 (f3)**]. This observation can be correlated with the MTS results discussed in the previous section of greater cell viability on the glycine NHS ester functionalized nanocomposites.

To better confirm about the cell adhesion, spreading and proliferation, 3T3 fibroblasts were cultured at lower concentration than that of the live/dead assay on the scaffolds as discussed above and stained with calcein AM after 24 h and 48 h of culture to monitor the changes in cell morphology with time. Quantitative analysis of cell morphology was carried out using confocal images of calcein AM stained cells seeded on different substrates for 24 h and 48 h [**Figure 5.27 (a)**], with relatively lower cell density so that analysis was restricted to only those cells, which were not in contact with more than one cell. **Figure 5.27 (b) & (c)**indicate that projected cell area and percent cell spreading were significantly higher for cells on glycine NHS ester functionalized nanocomposites compared to cells on the non-functionalized nanocomposites, at $p \leq 0.05$. Projected cell area for cells on functionalized nanocomposites is also significantly higher than the cells on TCP and Ch, at $p \leq 0.05$; whereas percent cell spreading for cells on modified nanocomposites, TCP and Ch are not significantly different. These observations demonstrate that adhesion, spreading and proliferation of 3T3 fibroblasts on glycine NHS ester functionalized nanocomposites occur more favorably compared to pristine nanocomposites. Quantitative analysis of cell density confirms better cell proliferation on glycine NHS ester functionalized nanocomposites owing to improved cell adhesion and spreading, than that on the non-functionalized nanocomposites. Cell densities, after cultured for 24 h and 48 h, on EFPAni:Ch-4 wt% (79 ± 22 and 156 ± 45) andEFPAni:Ch-6 wt%

(76 ± 28 and 137 ± 41) statistically differ from that of PAni:Ch-4 wt% (43 ± 17 and 71 ± 19) and PAni:Ch-6 wt% (48 ± 19 and 77 ± 18) at $p \leq 0.05$.However, cell densities on the controls (TCP and pure Ch) are not significantly different from that of the surface functionalized nanocomposites films.

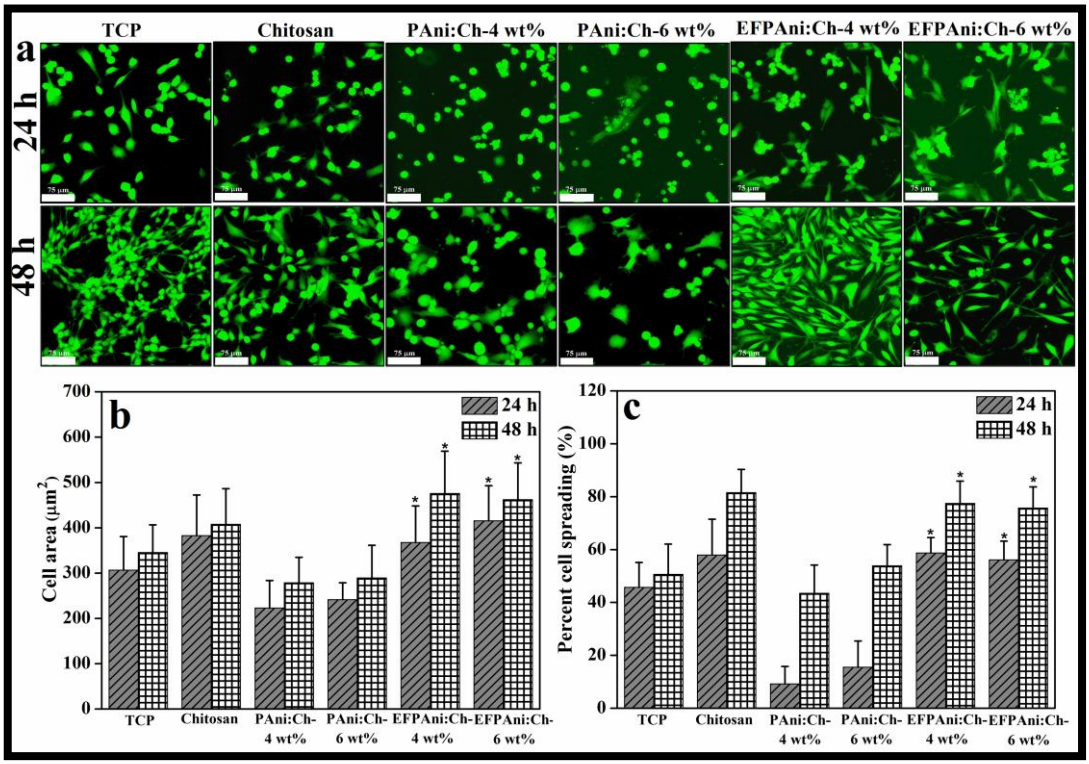

Figure 5.27. (a) Representative confocal images of calcein AM stained viable cells seeded on different scaffolds (labeled in the photographs) for 24 h and 48 h, used for analysis of cell morphology(Scale bar = 75 μm). (b) Histogram showing area covered by single cell on different scaffolds after 24 h and 48 h. c. Histogram of percent of cell spreading on different scaffolds after 24 h and 48 h. *indicates significant differences between the non-functionalized and functionalized nanocomposites at $p \leq 0.05$.

5.4.1.3.2 3T3 cell attachment

To further confirm the results described above, 3T3 cells cultured for 3 days on the non-functionalized and glycine NHS ester functionalized nanocomposites were characterized by SEM and shown in **Figure 5.28**. SEM images reveal that 3T3 cells cultured on glycine NHS ester functionalized nanocomposites adhere, spread and proliferate well forming clusters [**Figure 5.28 (c) & (d)**].

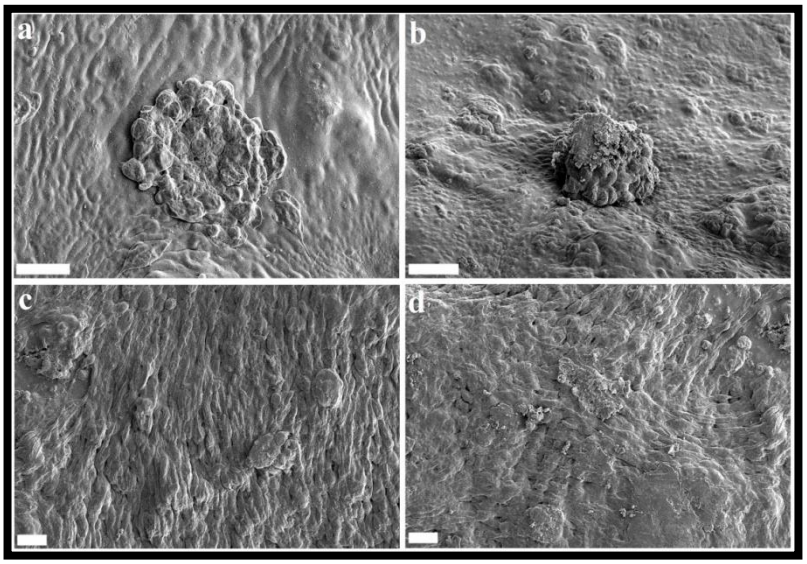

Figure 5.28. SEM images of 3T3 cells cultured for 3 days on the non-functionalized (a) PAni:Ch-4 wt%, (b) PAni:Ch-6 wt% and glycine NHS ester functionalized (c) EFPAni:Ch-4 wt% and (d) EFPAni:Ch-6 wt%.(Scale bar = 20 μm)

Regular cell alignment with spindle and elongated morphology of fibroblasts occur due to favorable adhesion on the materials surface confirming enhanced cell-biomaterial interaction. In contrast, cells seeded onto the non-functionalized nanocomposites [**Figure 5.28 (a) & (b)**] formed clusters but adopted round morphology indicating poor cell spreading and attachment. Although the nanofibers are randomly oriented, the cells started to align in some particular directions on the surface functionalized nanocomposites films with simultaneous formations of filopodia and lamellipodia-like extensions. This results suggest that the cells on surface functionalized nanocomposites interact well with the sacffold and started to migrate through the porous nanofibrous network. The different polar functionalities mainly carboxyl and amino groups on the glycine NHS ester functionalized meshes provides necessary binding sites to the integrin proteins on the cell surface resulting in the formation of focal adhesions. This accelerates the cell attachment, followed by cell spreading. In contrast, non-functionalized nanocomposites due to lack of bioactive binding sites show poor cell attachment and morphology as compared to surface functionalized nanocomposites. The observed cell attachment on the non-functionalized meshes may be due to the serum proteins adsorbed by the nanocomposites, which offer limited focal adhesions for cell attachment.

5.4.1.4 PC12 cell behaviour

5.4.1.4.1 Beta (III) tubulin immunochemistry

The PC12 cells were cultured for 7 days in differentiating medium on different PAni:Ch nanocomposites films with and without collagen I coating to investigate the suitability of these materials for neural tissue engineering. This cell line has been widely used as a model neuronal system. PC12 cells cultured with NGF (Nerve growth factor) develop long neurite outgrowth, become electrically excitable and take on many of the biochemical traits of sympathetic noradrenergic neurons [413]. Since, PC12 cells readily adhere to collagen, all the electrospun meshes were coated with collagen I. Collagen I is a fibril forming collagen present in the ECM of the peripheral nervous system (PNS) and plays an important role in the development of the peripheral nervous system as well as in the maintenance of normal peripheral nerve function during adulthood [414]. Immunolabelling with beta (III) tubulin antibody was performed to confirm PC12 cell differentiation into sympathetic neurons. The PC12 cells grown on the collagen I coated nanocomposites, glycine NHS ester functionalized and non-functionalized nanocomposites were labelled with beta (III) tubulin antibody to visualize cytoskeletal microtubules, which are dynamic polymer filaments of alpha and beta tubulin subunits that drive neurite outgrowth and control neuronal morphology [324].

Figure 5.29 (a1-b3) represents the confocal images of beta III tubulin stained PC12 cells cultured on different substrates after seven days to study the effect of surface functionalization and collagen coating of substrates on neuronal differentiation. It shows that PC12 cells are differentiated well only on collagen coated PAni:Ch nanocomposites. Cell numbers, counted from the numbers of DAPI-stained nuclei from confocal images, are 206 ± 52 (Collagen coated glass), 153 ±32 (Collagen coated PAni:Ch-4 wt%) and 146 ± 27 (Collagen coated PAni:Ch-6 wt%); whereas very poor cell adhesion has been observed on PAni:Ch-4 wt% (56 ± 21), PAni:Ch-6 wt% (43 ± 16), EFPAni:Ch-4 wt% (72 ± 20) andEFPAni:Ch-6 wt%(67 ± 24), with poor cell morphology in unhealthy organization in clustered form. The cell density on the collagen coated nanocomposites is significantly higher from that of uncoated nanocomposites (non-functionalized and functionalized nanocomposites) at $p \leq 0.05$.

However, statistical significance doesn't exist between the adherent cell numbers on collagen coated glass and PAni:Ch nanocomposites. This observation reveals that collagen coating affects adhesion of PC12 cells significantly and the surface functionalization by glycine NHS ester has no affect on PC12 cell adhesion.

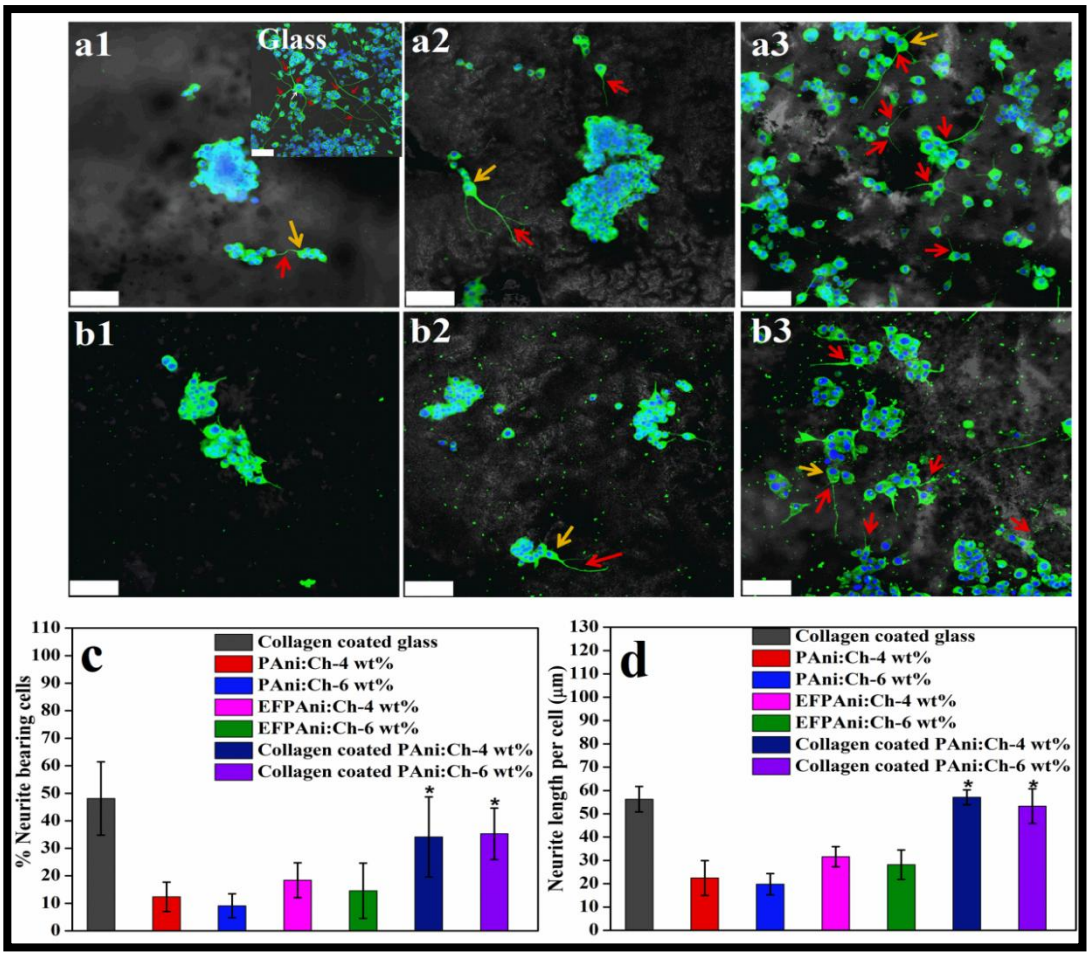

Figure 5.29. Beta (III) tubulin immunostaining of PC12 cells cultured for 7 days on non-functionalized PAni:Ch-4 wt% (a1) and PAni:Ch-6 wt% (b1), EFPAni:Ch-4 wt% (a2), EFPAni:Ch-6 wt% (b2) and collagen I coated PAni:Ch-4 wt% (a3) and PAni:Ch-6 wt% (b3) [Scale bar = 75 μm]. Inset of a1 shows the immnulabelling of PC12 cells cultured on collagen coated glass cover slip. Quantitative analysis of differentiated PC12 cells: (c) % neurite bearing cells and (d) average neurite length per cell.

Analysis of neurite formation shows that percent of neurite bearing cells on collagen coated PAni:Ch-4 wt% (34% ± 15), PAni:Ch-6 wt% (35% ± 9) are significantly greater that of uncoated PAni:Ch-4 wt% (12% ± 5), PAni:Ch-6 wt% (10% ± 4), EFPAni:Ch-4 wt% (18% ± 6) and EFPAni:Ch (15% ± 10) at $p \leq 0.05$ [**Figure 5.29 (c)**]. The average neurite length per cell as presented in **Figure 5.29 (d)** were as: 57 ± 4 μm (Collagen coated PAni:Ch-4 wt%), 53 ± 8 μm (Collagen coated PAni:Ch-6 wt%), 22 ± 7 μm (uncoated PAni:Ch-4 wt%), 19 ± 5 μm (uncoated PAni:Ch-6 wt%), 32 ± 5 μm (uncoated EFPAni:Ch-4 wt%) and 28 ± 6 μm (uncoated EFPAni:Ch-6 wt%). The results demonstrate that the average neurite lengths per cell on the collagen coated PAni:Ch nanocomposites films are statistically different from those of all uncoated nanocomposites films, at $p \leq 0.05$. However, there is no significant difference on neurite formation and neurite outgrowth on the collagen coated nanocomposites films and collagen coated glass.

5.4.1.4.2 PC12 cell attachment

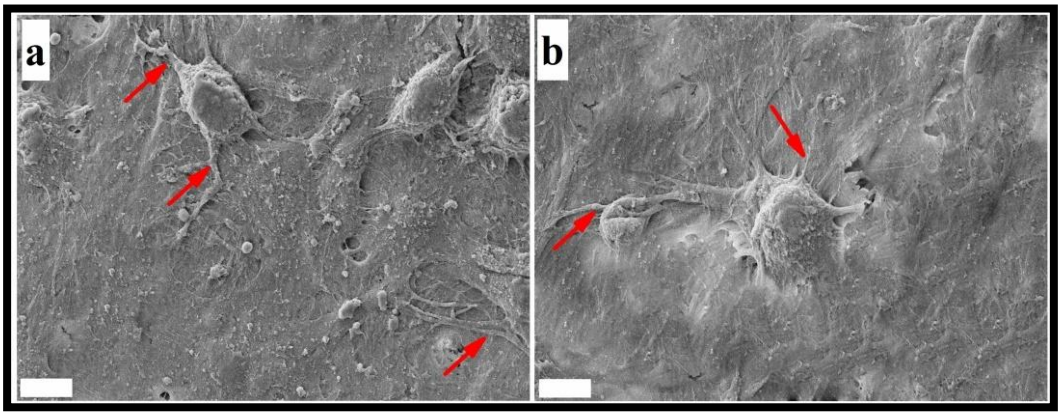

Figure 5.30. Scanning electron micrographs of PC12 cells after 7 days of culture on collagen coated (a) PAni:Ch- 4wt% and (b) PAni:Ch- 6wt%. Red arrows point to the neurite projection. Scale bar = 5 μm.

In order to confirm the PC12 attachment to study their morphology on the collagen coated nanocomposites, SEM of PC12 cells cultured on collagen coated PAni:Ch-4 wt% and PAni:Ch-6 wt% was performed and the corresponding micrographs are shown in **Figure 5.30**.The SEM images confirmed the results of the immunocytochemistry. All the nanocomposites films coated with collagen demonstrate attachment of PC12 cells with neurite projections [pointed in red in

Figure 5.30]. However, SEM did not show any cell attachment on uncoated nanocomposites (results are not shown). The observation suggests that collagen coated is essential for PC12 cell attachment, which is agreement with several earlier reports. The results also confirm that surface functionalization by glycine NHS ester is not sufficient to offer proper binding sites for PC12 attachment, unlike 3T3 fibroblasts as discussed in **Section 5.5.1.3**.

5.5 Electrical stimulation of PC12 cells

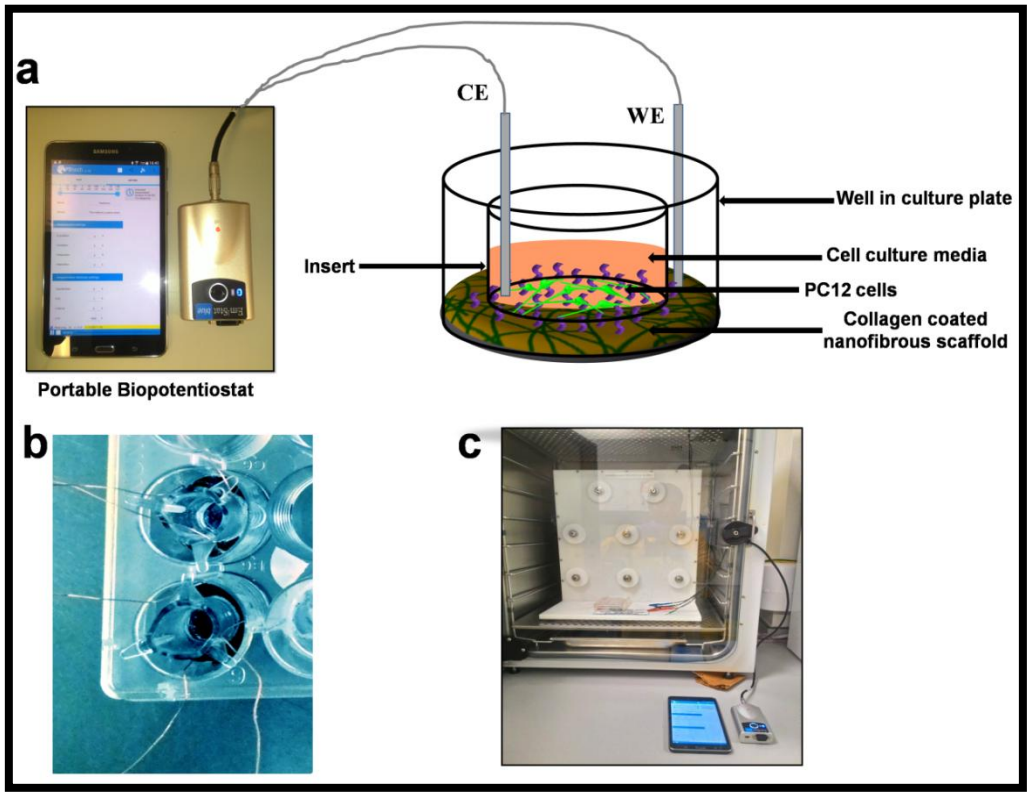

Figure 5.31. (a) Schematic illustration of the electrical stimulation experiment using a custom made electrical stimulation set up ; (b) photograph of self made cell culture plate with PAni:Ch nanocomposites with 4 wt% and 6 wt% PAni content (dark blue colur) fixed on it for electrical stimulation experiment; (c) photograph of the electrical stimulation experiment in situ.

The beta tubulin immunochemistry and cell adhesion test confirms the PC12 cell differentiation on collagen coated PAni:Ch nanocomposites. Besides, PAni:Ch nanocomposites are found to biocompatible and have the ability to support the cell functions as demonstrated in previous sections, the nanocomposites are also

electrically conductive as revealed by *I-V* measurement. Therefore, it is believed that PAni:Ch nanocomposites has the potential to act as an electrically conductive biomaterial scaffold for electrical stimulation of nerve cells. To explore that potential, electrical stimulation of differentiated PC12 cells was carried out though collagen coated PAni:Ch nanocomposites using bespoke electrical stimulation set up as shown in **Figure 5.31 (a-c)**.

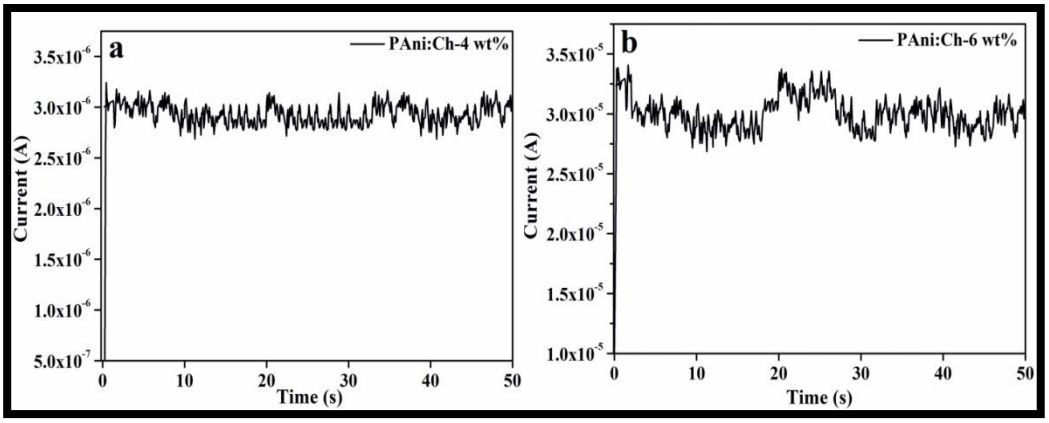

Figure 5.32. Current signal recorded (upto 50 s) during electrical stimulation of PC12 cells through conductive PAni:Ch nanocomposites through (a) collagen coated PAni:Ch-4 wt% and (b) collagen coated PAni:Ch-6 wt%. A constant potential of 500 mV/cm for 2 h was applied in chronoamperometric technique in pulsed mode (pulse duration 1 ms).

The detailed description of electrical stimulation set up and the experiment has been provided in **Chapter III [Section 3.6]**. Briefly, a constant electrical potential of 500 mV/cm was applied across the electrodes for 2 h/day for 3 consecutive days using a portable bipotentiostat (EmStat Blue, PalmSens BV, Netherlands) [**Figure 5.31 (a)**]. The electrical stimulation was carried out by a double pulsed potential chronoamperometric technique in an incubator [**Figure 5.31 (c)**]. Representative current signals during electrical stimulation of PC12 cells through the coated PAni:Ch-4 wt% and coated PAni:Ch-6 wt% are shown in **Figure 5.32 (a) & (b)**. For comparison, PC12 cells on coated PAni:Ch nanocomposites without electrical stimulation are also cultured under the same condition for 7 days treated as control.

For possible use as a smart stimuli responsive biomaterial scaffold for axonal regeneration in damaged nerves, electrical stimulation of differentiated PC12 cells

was carried out using collagen coated PAni:Ch-4 wt% and PAni:Ch-6 wt% as better neurite formation and outgrowth have been observed on them as demonstrated by preliminary beta (III) tubulin immunochemistry [**Subsection 5.4.1.4.1**]. Representative confocal images of the electrically stimulated and unstimulated PC12 cells on collagen coated various PAni:Ch nanocomposites are shown in **Figure 5.33(a1-b2)**. It appears from the confocal images that more neurite formation on electrically stimulated PC12 cells on collagen coated PAni:Ch nanocomposites as compared to the unstimulated PC12 cells. Therefore, the effect of electrical stimulation of PC12 cells through the conductive nanocomposites has been assessed in terms of quantitative analysis of percentage of neurite bearing cells, neurite per cell, neurite length per cell and median neurite lengths from the confocal images of beta tubulin stained PC12 cells on electrospun meshes and the results are shown in [**Figure 5.33(c-f)**].

Quantitative analysis indicates that electrical stimulation for 2 h/day for 3 consecutive days through conductive PAni:Ch nanocomposites scaffolds induces enhancement in the neurite formation and neurite outgrowth. The electrically stimulated PC12 cells have significantly greater number of neurite bearing cells on coated PAni:Ch-4 wt% (62% ± 13, N=388, m=318) and PAni:Ch-6 wt% (66% ± 17, N=413, m=356) when compared to the unstimulated cells on coated PAni:Ch-4 wt% (41% ± 10, N=364, m=209) and PAni:Ch-6 wt% (39% ± 8, N=359, m=194), at $p \leq 0.05$, where N and m denote number of cells and number of neurites analyzed [**Figure 5.33 (c)**]. Neurite lengths per cell and median neurite lengths of electrically stimulated cells on coated PAni:Ch-4 wt% (117 ± 23 and 70 ± 19 μm) and PAni:Ch-6 wt% (138 ± 36 and 73 ± 14 μm) were statistically different ($p \leq 0.05$) from unstimulated cells on coated PAni:Ch-4 wt% (61± 14 and 42±15μm), and PAni:Ch-6 wt% (55 ± 12 and 37 ± 12 μm) [**Figure 5.33 (d) & (e)**]. Analysis of neurites per cell reveals that each electrically stimulated PC12 cells has more number of neurites on coated PAni:Ch-4 wt% (1.85) and PAni:Ch-6 wt% (1.97) than those of unstimulated cells on coated PAni:Ch-4 wt% (1.16) and PAni:Ch-6 wt% (1.09) [**Figure 5.33 (f)**]. The results confirm that PC12 cells under electrical stimulation had more neurites per cell than those grown under no electrical stimulation and the results statistically different at $p \leq 0.05$. Ultimately, it can be concluded that that electrical stimulation of

PC12 cells through these conductive nanocomposites scaffolds has a beneficial effect on neurite formation and neurite outgrowth.

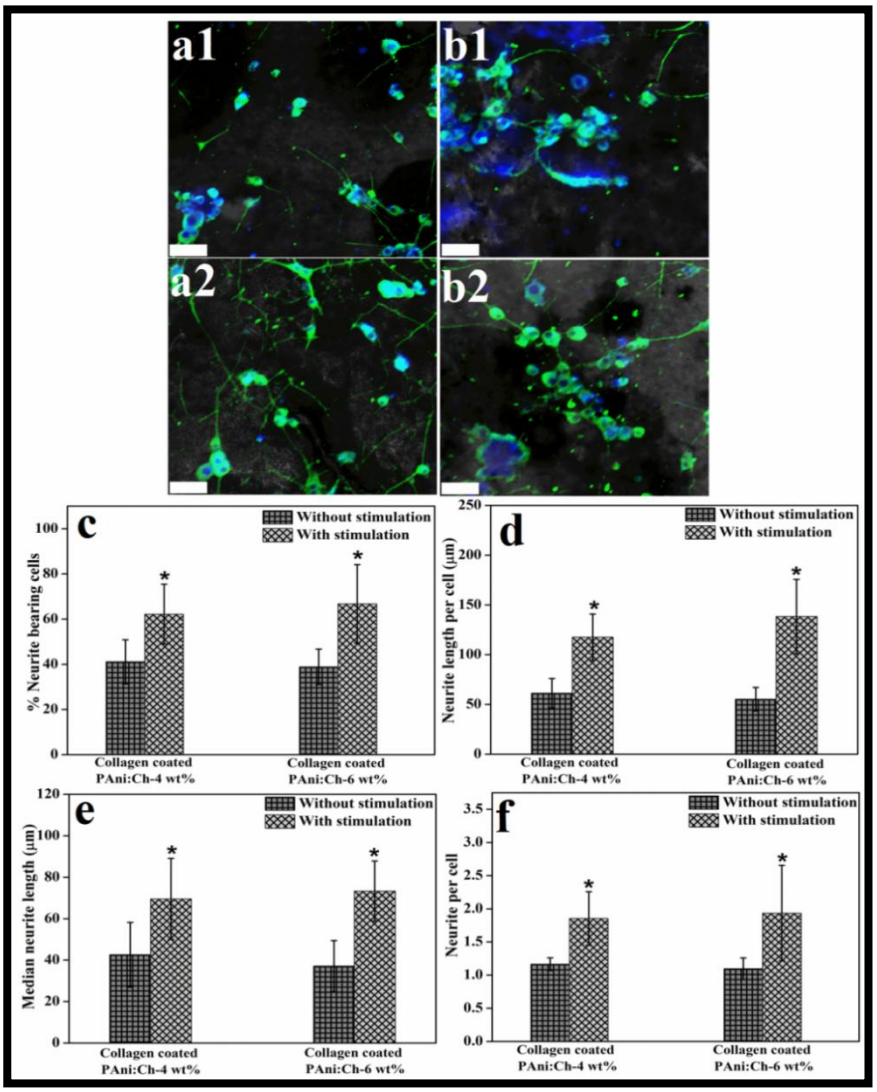

Figure 5.33. Confocal images with phase contrast overlay of beta (III) tubulin immunostained PC12 cells cultured for 7 days under no electrical stimulation (a1-collagen coated PAni:Ch-4 wt%, b1-collagen coated PAni:Ch-6 wt%) and under electrical stimulation of 500 mV/cm for 2h/day for 3 cosecutive days (a2-collagen coated PAni:Ch-4 wt%, b2-collagen coated PAni:Ch-6 wt%) [Scale bar = 75 μm]; (c) Percentage of neurite bearing cells, (d) Neurite length per cell, (e) Median neurite length and (f) Neurite per cell of differentiated PC12 cells on collagen coated PAni:Ch nanocomposites without electrical stimulation and with electrical stimulation. Data were Mean ± S.D. *indicates statistical significance difference from unstimulated PC12 cells at $p \leq 0.05$.

Moreover, it has been noticed that PAni:Ch-6 wt%, having lower sheet resistance as compared to that of PAni:Ch-4 wt%, provides improved differentiation of PC12 cells with more neurite bearing cells, neurite length per cell and median neurite length than those of PAni:Ch-4 wt%. Interestingly, this difference is statistically significant atp≤0.01. This significant change in neurite formation and neurite outgrowth on coated PAni:Ch-6 wt% under electrical stimulation is referred to the improved conductive behaviour of the nanocomposites due to higher conductive PAni content. It is also evident from the current signals during stimulation [**Figure 5.32**], which shows that more current flow through coated PAni:Ch-6 wt% (~30 μA) than PAni:Ch-4 wt% (~3 μA). This can be further correlated with the lower critical voltage (V_c) value for PAni: Ch-6 wt%, confirming the higher density of free charge carriers in all PAni:Ch-6 wt% than that of PAni:Ch-4 wt% as discussed in **Section 5.2.3**. Thus, the neurite formation and outgrowth increases with increase in current signal. Under electrical stimulation of 500 mV/cm, the availability of free charge carriers in PAni:Ch nanocomposites (more in PAni:Ch-6 wt%) offers more charge-transport between the scaffold and the cell membrane, resulting in the change in the resting membrane potential of differentiated PC12 cells. Consequently, the cell membrane undergoes an intensity-dependent depolarization resulting action potential, which is responsible for axonal growth. This change in cell membrane potential is also believed to activate growth-controlling transport processes across the plasma membrane and cause redistribution of cytoplasmic materials [120, 155, 196, 251, 415-417]. According to Patel *et al.*, ES causes electrophoretic accumulation of surface molecules on the working electrode (scaffold). All these are likely to be responsible for longer neurite growth or cell–substratum adhesion [415].

5.6 Summary

We have shown synthesis of PAni:Ch nanocomposites in contrast to previous studies which reported only composites of bulk PAni with Ch. SEM reveals interconnected networks of PAni nanofibers soaked in Ch matrix with rough and porous surface when compared to smooth pure Ch. Sheet resistance (R_s) calculations derived from I-V characteristics reveal no significant change in the conductive properties of the glutaraldehyde functionalized and glycine NHS ester functionalized nanocomposites from their non-functionalized counterparts and suggest that surface functionalization has been performed without much affecting the conductive properties of the

nanocomposites. The mechanical strength test reveals that tensile strengths of all the nanocomposites match the tensile strength of softer tissues. Stability test demonstrates that after incubation in physiological solution (PBS, pH=7.4) for 15 days, the nanocomposites reveal remarkable enhancement in porous morphology on the surface due to degradation of Ch matrix as confirmed from SEM analysis, whereas surface resistivity measurement reveals no significant change in conductive properties indicating no degradation occurs to PAni nanofibers in the nanocomposites. The distribution of pore diameters after 15 days of incubation in PBS has been increased from 20-100 nm to 50-1000 nm, providing the essential porosity of tissue engineered scaffolds. Therefore, we speculate that PAni nanofibers take a lead role in maintaining the electrical and structural stability of the nanocomposites as compared to Ch.

Incorporation of aldehyde functionality on the surface of PAni:Ch nanocomposites after functionalization by glutaraldehyde has been confirmed from FT-IR and XPS results. The FT-IR and XPS results suggest incorporation of aldehyde functionality in two possible ways: firstly, through amide bond formation between the amino group of Ch in PAni:Ch nanocomposites and aldehyde group of monomeric glutaraldehyde; secondly, through Schiff base formation between aldehyde group of monomeric glutaraldehyde and primary amine of Ch in the nanocomposites. The possible functionalization mechanisms have been proposed on these results and shown in **Figure 5.11**. Similarly, surface functionalization of PAni:Ch nanocomposites has been accomplished using BOC glycine NHS ester. Incorporation of glycine onto the surface of PAni:Ch nanocomposites has been confirmed in two ways: by interaction with the carboxylic acid site of glycine keeping the amine site free and vice versa as confirmed from FT-IR and XPS results. Probable interaction mechanisms between unprotected glycine NHS and the nanocomposite surface have been also proposed based on FT-IR and XPS results and shown in **Figure 5.13**. Contact angle analysis by OWRK and AB method indicates improvement in wettability and surface polarity of the nanocomposite after surface functionalization glutaraldehyde and glycine NHS ester. OWRK method demonstrates enhancement in total surface energy (γ_s), polar component of surface energy (γ_s^p) and percentage of surface polarity of PAni:Ch nanocomposites after surface functionalization glutaraldehyde and glycine NHS ester. Similar observation has been also confirmed from AB method. In fact, AB method further confirm the FT-IR and XPS results by

demonstrating in the enhancement of the Lewis basic (γ_s^-) component of surface energy of the nanocomposites due to basic aldehyde incorporation after surface functionalization by glutaraldehyde, whereas the enhancement in the Lewis acid (γ_s^+) component of surface energy of the glycine NHS ester functionalized nanocomposites indicates the incorporation carboxylic acid functionality on the surface.

The glutaraldehyde functionalized nanocomposites exhibit higher urease activity immobilized on it owing to improved surface hydrophilicity due to the incorporation of polar aldehyde (-CHO) and hydroxyl (-OH) functionality when compared to its non-functionalized counterpart. The Michaelis constant (K_m) has been determined to be 5.41 mM, 13.93 mM and 21.5 mM from the Lineweaver-Burk plot for free and immobilized urease on glutaraldehyde treated and untreated films, respectively, indicating improved kinetics of urease immobilized on glutaraldehyde functionalized nanocomposites.

Both types of surface functionalized nanocomposites demonstrate very less hemolytic activity (less than 5%) when compared to the non-functionalized counterparts, indicating improved blood compatibility of the materials. MTS proliferation assay reveal significant improvement in MDA-MB-231 cell viability on glutaraldehyde functionalized nanocomposites. Furthermore, MDA-MB-231 cell seeded on glutaraldehyde functionalized nanocomposites exhibit significantly higher percentage of viability, adhesion, spreading and morphology as confirmed after AO/EtBr staining and cell adhesion test by SEM. MTS proliferation assay indicates the improved viability of 3T3 fibroblasts and a neuronal rat pheochromocytoma (PC12) cells on glycine NHS ester functionalized nanocomposites, indicating their non-cytotoxic effect. Surface functionalized nanocomposites demonstrate improved 3T3 cell adhesion, spreading, proliferation and morphology as confirmed by calcein-AM/ethidium homodimer live/dead assay and SEM analysis. The study further demonstrates that several factors such as surface functional groups and charge as well as wettability and material stiffness, can be moderated by surface functionalization of PAni:Ch nanocomposites with polar functional groups to improve cell adhesion, spreading, and growth on conductive PAni based biomaterials. The collagen coated PAni:Ch nanocomposites support the growth and differentiation of PC12 cells to sympathetic neurons comparable to control collagen-coated glass plate. Electrical stimulation of PC12 cells under potential of 500 mV/cm for 2h/day through the

conductive collagen coated PAni:Ch nanocomposites demonstrates more neurite formation and longer neurite outgrowth than the unstimulated cells on the same scaffolds and indicates PAni:Ch nanocomposites may be suitable as conductive scaffold for nerve repair. It has been observed that collagen coated PAni:Ch-6 wt% with better conductivity, provides improved differentiation of PC12 cells with more neurite bearing cells, neurite length per cell and median neurite length than those of PAni:Ch-4 wt% with lower conductivity.

The results indicate that electrically conductive PAni:Ch nanocomposites offer a new scaffold for tissue engineering applications. Currently, these materials match the tensile strength of softer tissues providing potential in nerve repairing applications. Optimization of parameters could create a stiffer substrate providing additional possibilities for bone and cartilage tissue engineering.